Gadolinium Endohedral Metallofullerenes for Future Magnetic Resonance Imaging Contrast Agents

Youqing Ye

Dissertation submitted to the Faculty of Virginia Polytechnic Institute and State University in partial fulfillment of the requirements for the degree of

Master in Science

In

Chemistry

Harry C. Dorn

Harry W. Gibson

Lesley E. LaConte

Key words: Endohedral Metallofullerene, Trimetallic Nitride Template, Magnetic Resonance Imaging, Relaxivity, Contrast Agent

Gadolinium Endohedral Metallofullerenes for Future Magnetic Resonance Imaging Contrast Agents

Youqing Ye

Abstract

Gadolinium endohedral metallofullerenes (EMFs) have shown the potential to become next generation magnetic resonance imaging (MRI) contrast agents due to their significantly improved efficiency and safety, as well as multi-day body retention which allows for a longer surgery and observation compared to current contrast agents. In Chapter 1, I have reviewed the development of gadolinium EMF based MRI contrast agents. In Chapter 2, I have described my study of $Gd_3N@C_{80}$ and $Gd_3N@C_{84}$ metallofullerenols as next generation MRI contrast agents. The metallofullerenols are synthesized and characterized utilizing UV-vis, IR, X-ray photoelectron spectroscopy (XPS) and dynamic light scattering (DLS). In addition, relaxivity data and the observation of magnetic resonance images of the samples at different concentrations showed that $Gd_3N@C_{84}$ metallofullerenol had enhanced relaxivity compared to $Gd_3N@C_{80}$ metallofullerenol. The enhanced relaxivity was attributed to the special "egg shape" of the $Gd_3N@C_{84}$ cage. In Chapter 3, I have described the relaxivity study of $Gd_3N@C_{80}$ (without functionalization) in oleic acid, which could be used as an MRI contrast agent for more hydrophobic bioenvironments. The results show that $Gd_3N@C_{80}$ has a reasonable relaxation effect (relaxivity ~10 $mM^{-1}S^{-1}$ at 1.4 T) in oleic acid and could be a viable contrast agent even without functionalization. In Chapter 4, I have discussed the outlook of gadolinium EMF-based MRI contrast agents and suggested several directions for future work.

Acknowledgement

I would like to take this opportunity to thank my advisor, Professor Harry C. Dorn. He guided me into the exciting world of endohedral metallofullerenes and provided me the opportunity to explore this area. Needless to say, I have benefited from the instruction and advice from him. He is a renowned scientist, but he is always patient to help me on fundamental questions and in the smallest details. Also, I see in him a scientist who is never satisfied with his current accomplishment, but is always curious about the next puzzle in the field. I appreciate him as a knowledgeable advisor and a respectful role model, and I will carry what I gained in his group throughout my life.

I also thank Professor Harry W. Gibson, Professor Louis A. Madsen, Professor Lesley E. LaConte. They spent extra time to serve as my graduate committee, and the help and suggestions I received from them are very much appreciated. I also benefited from the graduate courses I took at Virginia Tech, and I would like to thank the instructors, Professor James E. McGrath, Professor Paul R. Carlier, Professor Alan R. Esker, Professor Tijana J. Grove, and Professor Louis A. Madsen. I also thank Professor Patricia G. Amateis and Ms. Victoria Long, who trained me as a qualified teaching assistant.

I have been receiving extensive help from the colleagues in the Dorn research group. I enjoyed working with group alumni Dr. Jianyuan Zhang, Professor Timothy Fuhrer, Professor James C. Duchamp, Christopher Pregot, and current group members Tinghui Li, Boris F. Kiselev, Kanwarpal (“Paul”) S. Bakshi, Hunter Champion, Professor Libin Bai, Professor Haijun Wang and Professor Xinwu Ba. In addition, I am grateful for the numerous helps from our administrative assistant, Stephanie J. Hurt.

I also thank the collaborators outside our group. Especially, Chapter 2 represents an extensive collaboration, and herein I thank Professor Louis A. Madsen, Professor John R. Morris, Professor Stephan M. LaConte, Ying Chen, Sharavanan Balasubramaniam, David H. Hobert, Yafen Zhang for their generous help. I thank Dr. Michael D. Shultz and Dr. Jeffery L. Parks for their training on ICP-MS measurements. I also thank all the helpful professors, administrative staff, technicians and classmates at Department of Chemistry at Virginia Tech and the Virginia Tech Carilion Research Institute (VTCRI). I will forever value the memories at Virginia Tech.

Finally I want to thank the continuing support from my parents at China. Their love is the most important impetus for me to live a wonderful life.

Table of Contents

List of Figures

List of Tables

Chapter 1 Background Overview

1.1 Biomedical applications of Gd endohedral metallofullerenes

Nanomaterials have provided promising new opportunities in the development of new pharmaceutical agents. As a special family of nanomaterials, endohedral metallofullerenes (EMFs) have attracted extensive scientific attention in the last two decades.[1] Endohedral metallofullerenes are fullerene cages with metal ions or clusters inside. In EMFs, the spherical cages can encapsulate metal atoms or clusters that have diagnostic or therapeutic effects, and they also function as the protectors and carriers of the metal atoms or clusters: on one hand the carbon cages are stable *in vivo* to prevent the toxic encapsulated species from being released to or reacting with the biological surroundings; on the other hand, they still have enough reactivity for functionalization which can tune their solubility, biological behavior, or *in vivo* targeting. Therefore, EMFs are widely developed as diagnostic and therapeutic materials.

EMFs are fullerenes with metallic atoms or clusters inside the cage.[1] Based on the endohedral contents, they can be categorized into monometallic,[2] dimetallic,[3] trimetallic nitride template,[4] metal carbide,[5] metal oxide,[6] metal sulfide,[7] metal cyanide EMFs,[8] with a few exceptions. The metal elements that have been encapsulated include Sc, Y, Ti, and most lanthanide metals. Among these metals, Gd has 7 unpaired f-orbital electrons in its ionic form, Gd^{3+}, and therefore has significant paramagnetism which enables it to be used as magnetic resonance imaging (MRI) contrast agent. Due to the toxicity of Gd^{3+}, in current commercial contrast agents, Gd^{3+} ions are used in relatively stable chelation complexes, as seen in the examples in Figure 1.

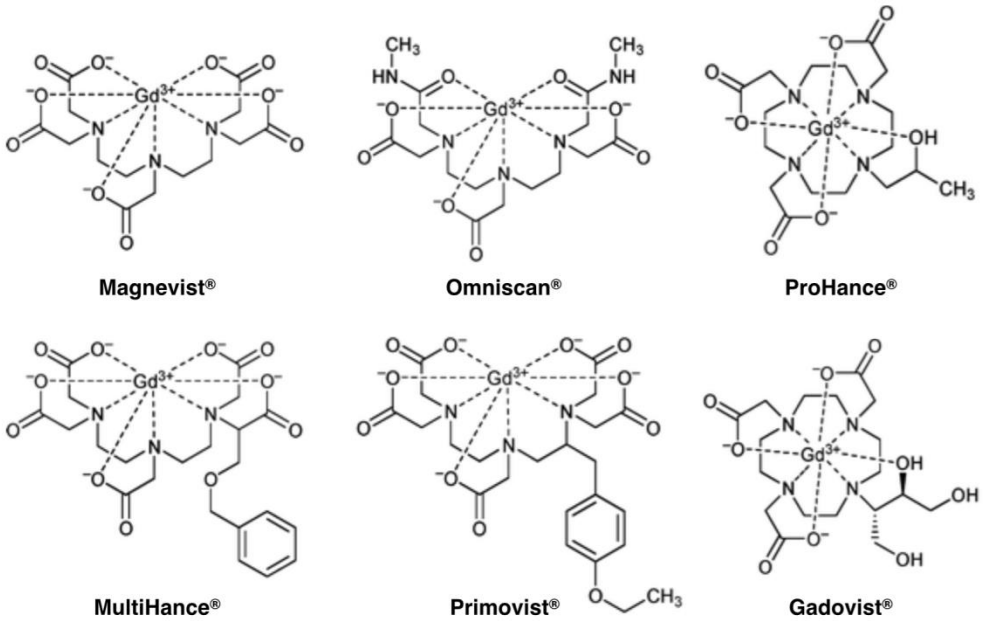

Figure 1. Common commercial gadolinium based MRI contrast agents.

However, it has been found that these commercial agents can still suffer from Gd^{3+} release from the chelating ligands. The FDA requested a risk warning on gadolinium based MRI contrast agents in 2007,[9] since it was suggested that the use of these agents had a high correlation with a debilitating skin disease, nephrogenic systemic fibrosis (NSF). Therefore, a safer MRI contrast agent is clearly needed.

As early as 2001, a gadolinium-based EMF was functionalized with hydrophilic groups for use as a MRI contrast agent by the Shinohara group.[10] They introduced hydroxyl groups to the monometallic EMF $Gd@C_{82}$ with tetrabutylammonium hydroxide (TBAH) or crown ether as a phase transfer catalyst (Figure 2). The functionalized derivative, $Gd@C_{82}(OH)_n$, exhibited very high relaxivity (81 $mM^{-1}S^{-1}$ at 1.0 T, compared to 3.9 $mM^{-1}S^{-1}$ for Magnevist at the same condition). In addition, the closed carbon cage provided excellent protection from gadolinium release. The same functionalization approach was later used in several other lanthanide-based EMFs.[11]

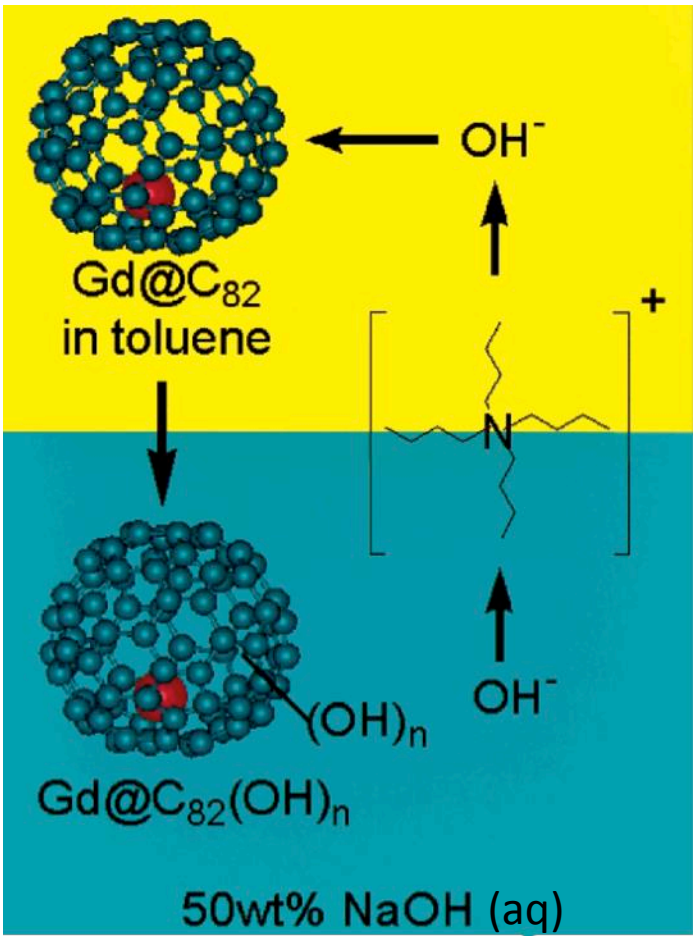

Figure 2. Phase transfer catalyzed hydroxylation of $Gd@C_{82}$.

Since these initial studies, many reports focusing on EMF based MRI contrast agents were published. The Wilson group functionalized monometallic $Gd@C_{60}$ via both hydroxylation and Bingel reactions.[12,13] At the same time, the aggregation behavior[13] and the pH-response behavior[14] of these functionalized EMFs were also studied by the same group. It has been established that the high relaxivity of the EMF derivatives is directly related to the formation of large aggregates. Recently, a new functionalization method utilizing hydrogen peroxide and ammonia water was reported[15] to yield amino group-containing derivatives, which have an average formula of $Gd@C_{82}O_{14}(OH)_{14}(NH_2)_6$.

Trimetallic nitride template endohedral metallofullerenes (TNT EMFs) represent a special and very promising class of EMFs. The first TNT EMF, discovered in 1999 by the Dorn group, which consists of a triangle planar trimetallic nitride cluster inside a highly symmetric I_h-C_{80} fullerene cage (Figure 3), was determined to be $Sc_3N@I_h$-C_{80} (Figure 3)[4]. It had very high yield (7% of total soluble content in electric-arc synthesis upon discovery,[4] improved further during the recent decade[1]) that was only second to empty cage fullerene C_{60} and C_{70}, and much higher than any traditional monometallic or dimetallic EMF.

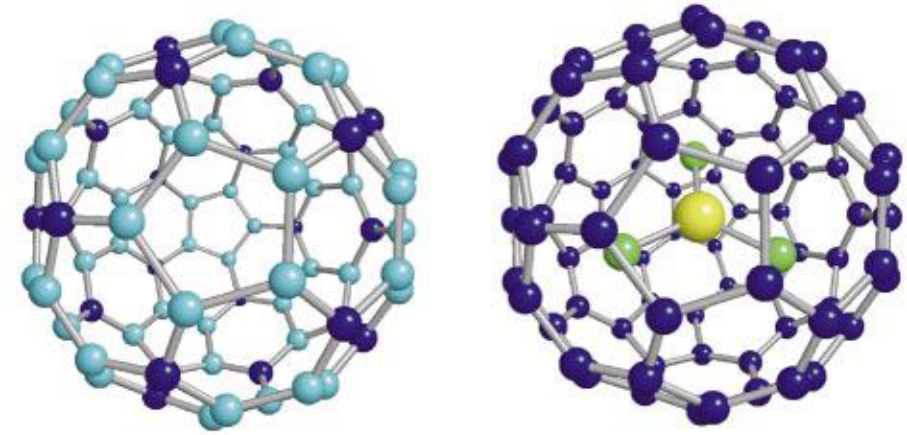

Figure 3. I_h-C_{80} fullerene cage and the first TNT EMF, $Sc_3N@I_h$-C_{80}.

Soon after, a second isomer, $Sc_3N@D_{5h}$-C_{80},[16] a smaller TNT EMF, $Sc_3N@D_{3h}$-C_{78},[17] and one of the first fullerene cages with the pentalene motif, $Sc_3N@D_3$-C_{68},[18] were discovered in the soot mixture from the same synthetic procedure. The pentalene motif (fused pentagons) in this molecule suggests that metallofullerenes do not necessarily obey the so-called isolated pentagon rule (IPR) for empty fullerenes,[19] which makes $Sc_3N@D_3$-C_{68} an earliest example of "non-IPR" fullerene cage. A wide range of other metals including Y, Gd, etc. has been encapsulated in TNT EMFs (Figure 2), as documented in several reviews.[20-22]

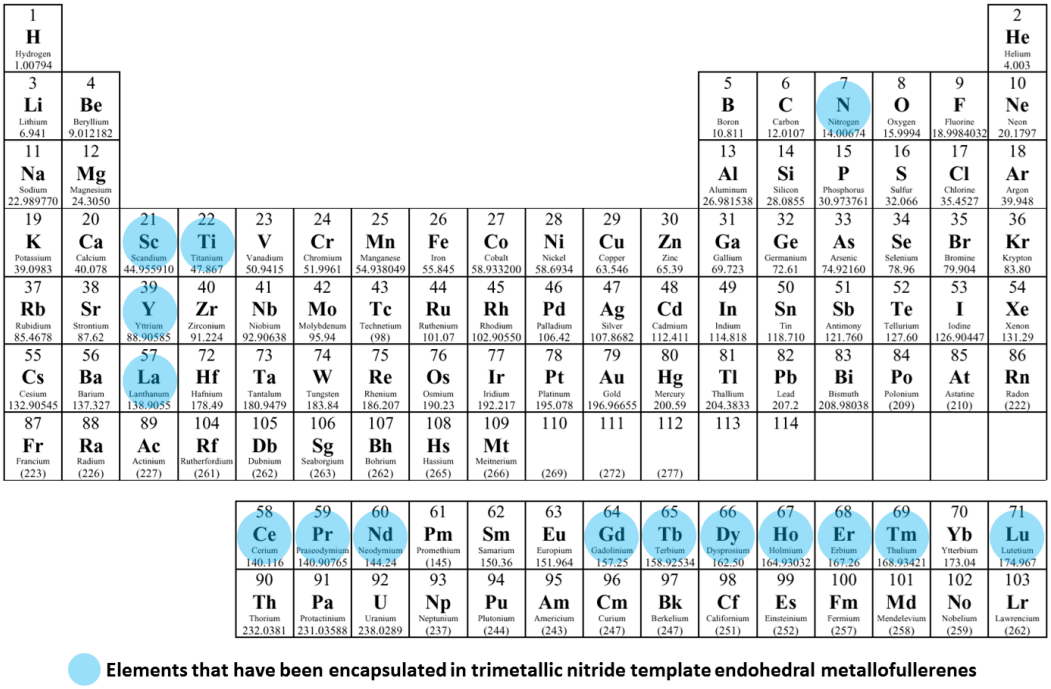

Figure 4. Elements that have been encapsulated in TNT EMFs. Figure reprinted with permission from ref. 20.

Among these metals encapsulated in TNT EMF, gadolinium is the one that is very important to MRI applications, as there are several advantages. First, the relatively high yield of TNT EMFs can significantly boost the practicability of commercial EMF-based MRI contrast agents. Second, TNT EMFs are more stable than empty fullerenes C_{60}, C_{70}, and monometallic EMF Gd@C_{82}, more soluble than monometallic Gd@C_{60}. These features will make it possible for long-term storage of these derivatives, as well as a reliable, safe cage protection in the biological environment. Third, TNT EMFs have three gadolinium ions as opposed to one or two, encapsulated in the fullerene cage and thereby exhibit higher molar magnetic moments.

The structure of $Gd_3N@I_h$-C_{80} was elucidated by the Stevenson group,[23] and its derivatives were soon used as an MRI contrast agents. In 2005, Gibson, Dorn, Fatouros and coworkers synthesized the first water-soluble $Gd_3N@C_{80}$ with hydrophilic poly(ethylene glycol) (PEG)

chains (MW=5000) and hydroxyl groups (Figure 3).[24] The *in vivo* MRI results illustrated in Figure 4 demonstrate the different distribution characteristics of a conventional commercial contrast agent (gadodiamide, 0.5 mmol/L, left hemisphere) and $Gd_3N@C_{80}[DiPEG5000(OH)_x]$ (0.013 mmol/L, right hemisphere) infused into a normal rat brain by means of a concurrent bilateral infusion, shown in successive T1-weighted MR images. As both the visual inspection (with over 40 times difference in concentration) and signal intensity profiles through the infusion sites demonstrate, the gadodiamide completely disappeared within three hours from the start of the infusion, compared with the $Gd_3N@C_{80}[DiPEG5000(OH)_x]$, which diffuses very slowly and, for the normal brain, appears to remain in the vicinity of the infusion catheter tip.[24]

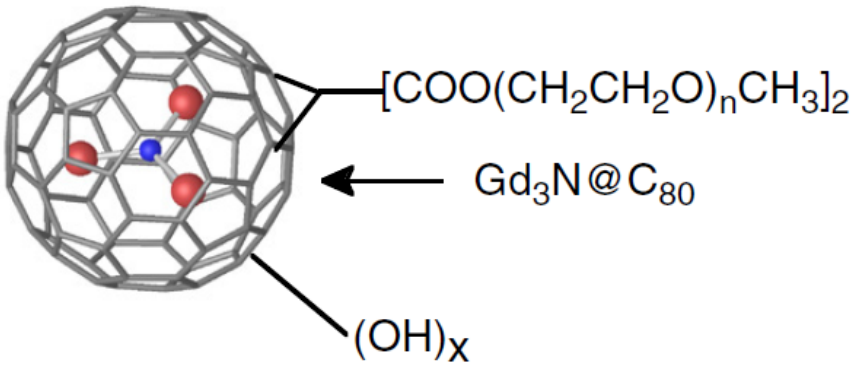

Figure 5. The first water-soluble $Gd_3N@C_{80}$ derivative.

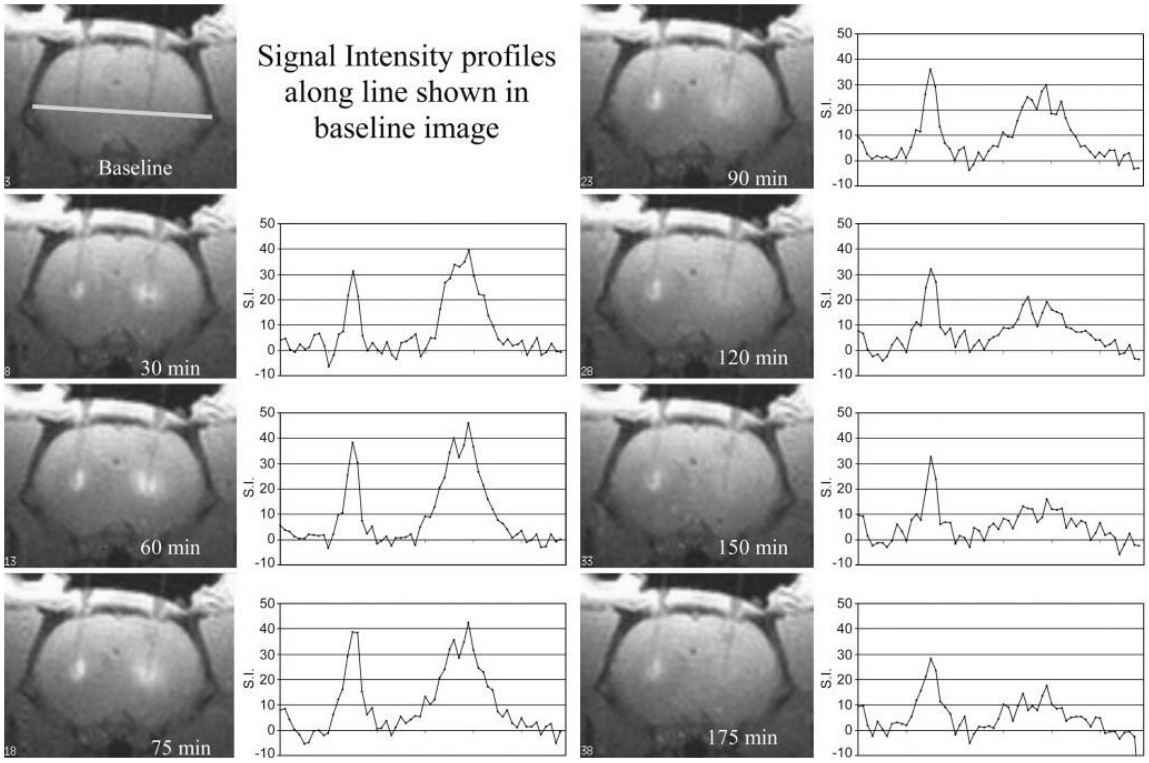

Figure 6. The T_1-weighted 2.4 T MR images (700/10) of bilateral infusion into a normal rat brain of 0.0131 mmol/L $Gd_3N@C_{80}$[DiPEG5000$(OH)_x$] and 0.5 mmol/L gadodiamide at a 0.2 L/min infusion rate, left and right side of image, respectively.

The relationship between the PEG chain length and the relaxivity of the functionalized $Gd_3N@C_{80}$ was further substantiated by the Dorn group in 2010.[25] In this work, PEG chains with molecular weights of 350, 750, 2000 and 5000 were introduced onto $Gd_3N@C_{80}$ via the Bingel reaction. From the dynamic light scattering data (Figure 5), it was concluded that longer PEG chains led to smaller aggregates. Large aggregate size can lead to significantly longer rotational correlation time of the contrast agents, which is the key reason for metallofullerene derivatives (10-250 nm aggregate size) have much higher relaxivities compared to commercial contrast agents (Figure 1) that generally do not form aggregates[26] (diameter less than 1 nm). Consistent

with this view, the relaxivity values at 0.35 T, 2.4 T and 9.4 T all increased with decreasing chain length.

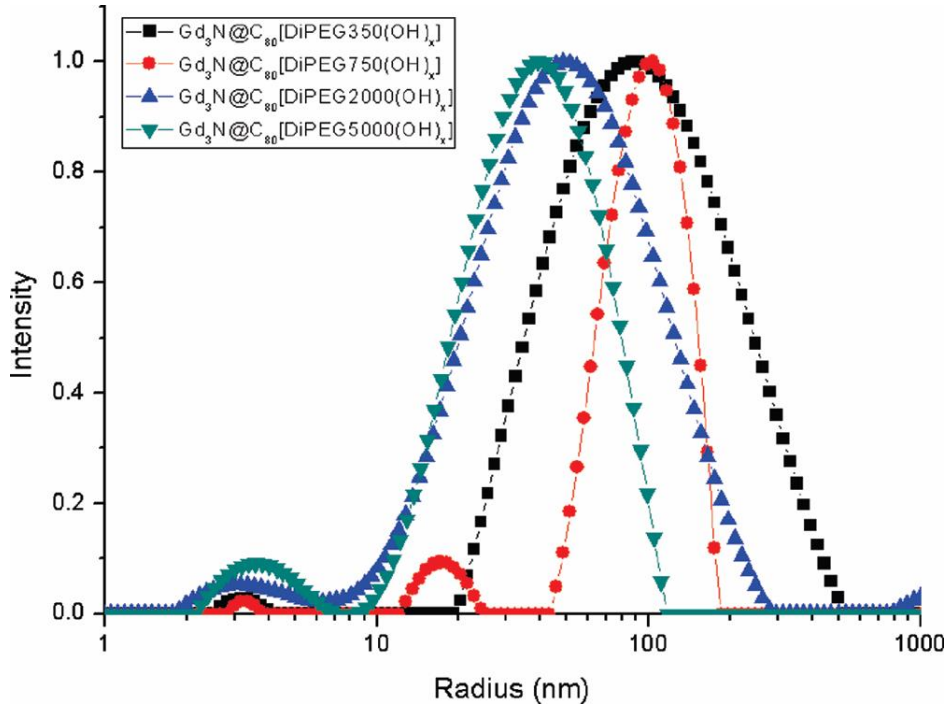

Figure 7. Dynamic light scattering data for $Gd_3N@C_{80}$ with PEG chains of different length.

Another important approach for making water-soluble $Gd_3N@C_{80}$ was developed by the same team in 2009.[27] The procedure (Figure 5) started with a free radical reaction with succinic acid acyl peroxide and then sodium hydroxide solution was used to introduce hydroxyl groups, to give the product, $Gd_3N@C_{80}(CH_2CH_2COOM)_{16}(OH)_{26}$. The scandium counterpart of the product was characterized by ^{1}H NMR and ^{13}C NMR, and the formula of the product, $Gd_3N@C_{80}(CH_2CH_2COOM)_{16}(OH)_{26}$, represented an average of a mixture determined by X-ray photoelectron spectroscopy (XPS).

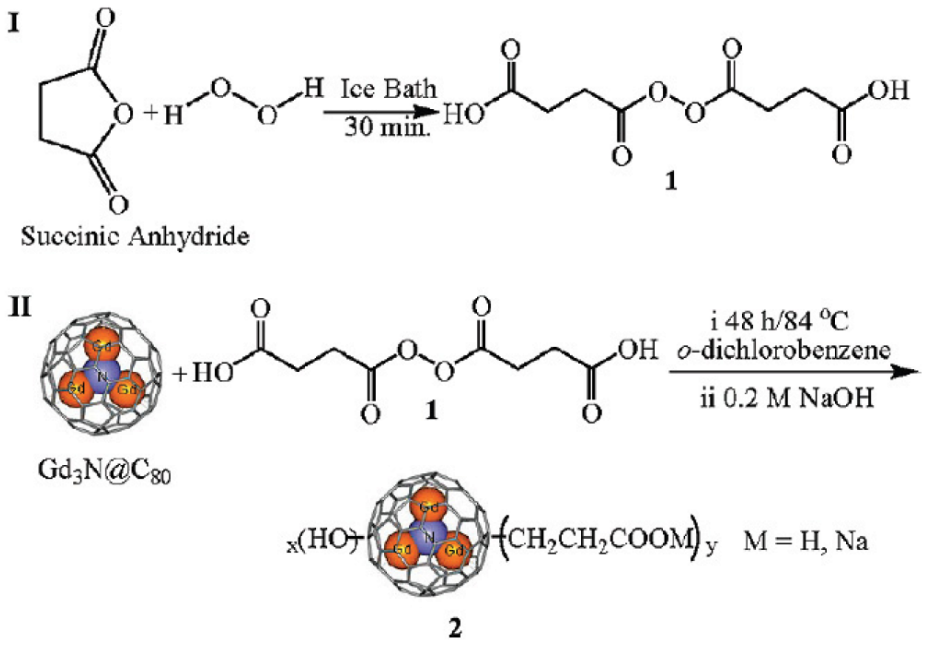

Figure 8. Functionalization of $Gd_3N@C_{80}$ with succinic acid aycl peroxide.

The functionalized $Gd_3N@C_{80}$ exhibited r_1 ($1/T_1$) relaxivity as high as 207 $mM^{-1}S^{-1}$ at a clinical field strength of 2.4 T,[27] which corresponds to a very effective MRI contrast agent. As shown in Figure 6a, the functionalized $Gd_3N@C_{80}$ gives much brighter images (left column) than the Omniscan contrast agent (right column) at a 30 times higher concentration. However, the high relaxivity is dependent on the aggregation of the fullerene cages. In phosphate buffer solutions (PBS) which is similar to the real biological environment, the salt effect caused disassembly of the aggregates, so the relaxivity values were lower and the corresponding images (Figure 6a, middle column) were not as bright. Figure 6b shows the *in vivo* study obtained by directly infusing the functionalized $Gd_3N@C_{80}$ solution into the brain of a rat. The results showed that the MRI contrast efficiency can last for several days post-infusion.

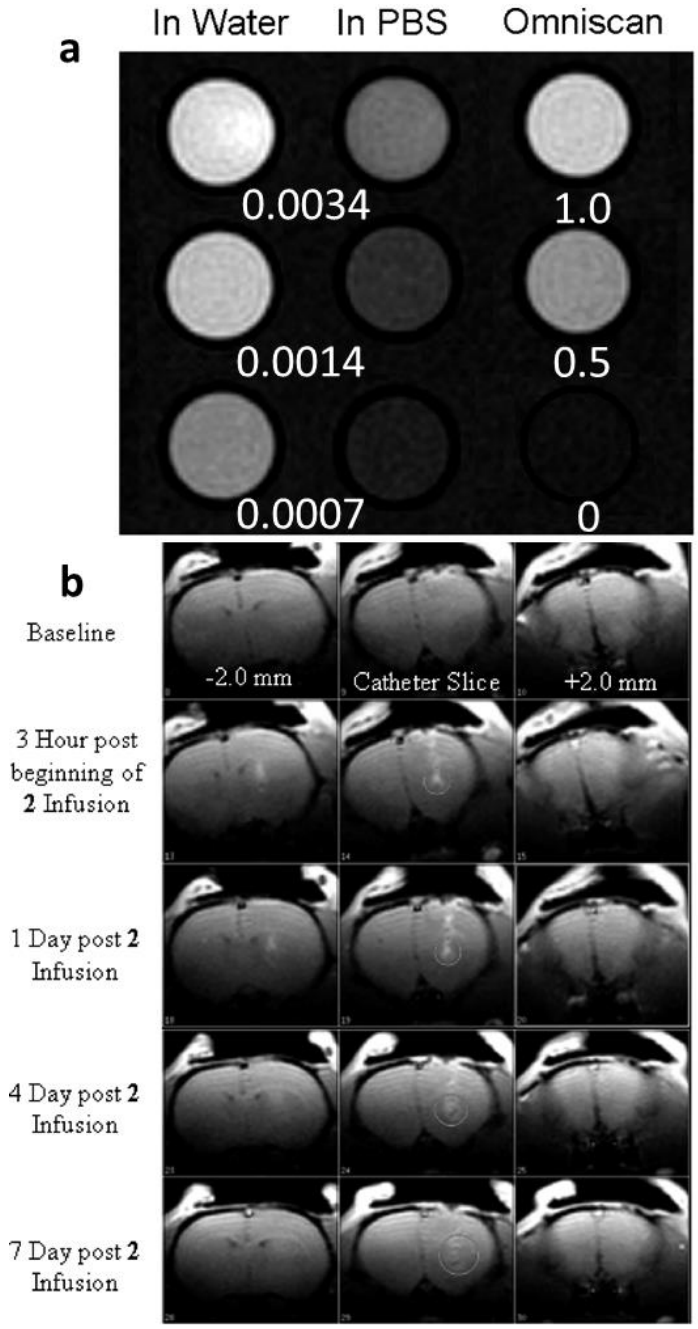

Figure 9. *in vitro* (a) and *in vivo* (b) T_1 weighted MRI images with functionalized $Gd_3N@C_{80}$ as contrast agent. In (a) the concentration (in mM) of functionalized $Gd_3N@C_{80}$ in water and PBS and Omniscan in water are marked below each spot. In (b) the direct infusion into T9 tumor-bearing rat brain of 0.0475 mM functionalized $Gd_3N@C_{80}$ was applied for 120 min at 0.2 μL/min.

One clear advantage of this agent is the introduction of the carboxyl groups which can be further conjugated with the amino groups of peptides or proteins for further biological purposes. For example, the agent can be further conjugated to peptide IL-13 to afford a bifunctional therapeutic and diagnostic ("theranostic") nano platform.[28,29]

With increasing attention from the biomedical community gadolinium EMF-based biomedicines are under rapid development, which are covered by several recent prospects and reviews.[1,30,31]

1.2 Development of gadolinium based EMFs

At the same time that $Gd@C_{82}$, $Gd@C_{60}$ and $Gd_3N@C_{80}$-based MRI contrast agents were under development, researchers were also gaining knowledge about other gadolinium based EMFs.[1] In 2008, another member of the TNT EMF family, $Gd_3N@C_s(51365)\text{-}C_{84}$, was determined by single crystal analysis to have the same special egg-shaped non-IPR fullerene cage[32] as in previously reported $Tb_3N@C_{84}$.[33] Soon afterwards, another two non-IPR EMFs, $Gd_3N@C_s(39663)\text{-}C_{82}$,[34] $Gd_3N@C_2(22010)\text{-}C_{78}$[35] and an IPR EMFs, $Gd_3N@D_3(19)\text{-}C_{86}$[36] were unambiguously elucidated by single crystal analysis. These structures are shown in Figure 10, with the fused pentagons highlighted in red color. Something notable is that although most fullerene cages obey the IPR, it is very common for gadolinium TNT EMFs to violate it. Recently the Dorn group suggested that these "pentalene containing" TNT EMF exhibit an enhanced dipole moment that will give special characteristics to these molecules.[37]

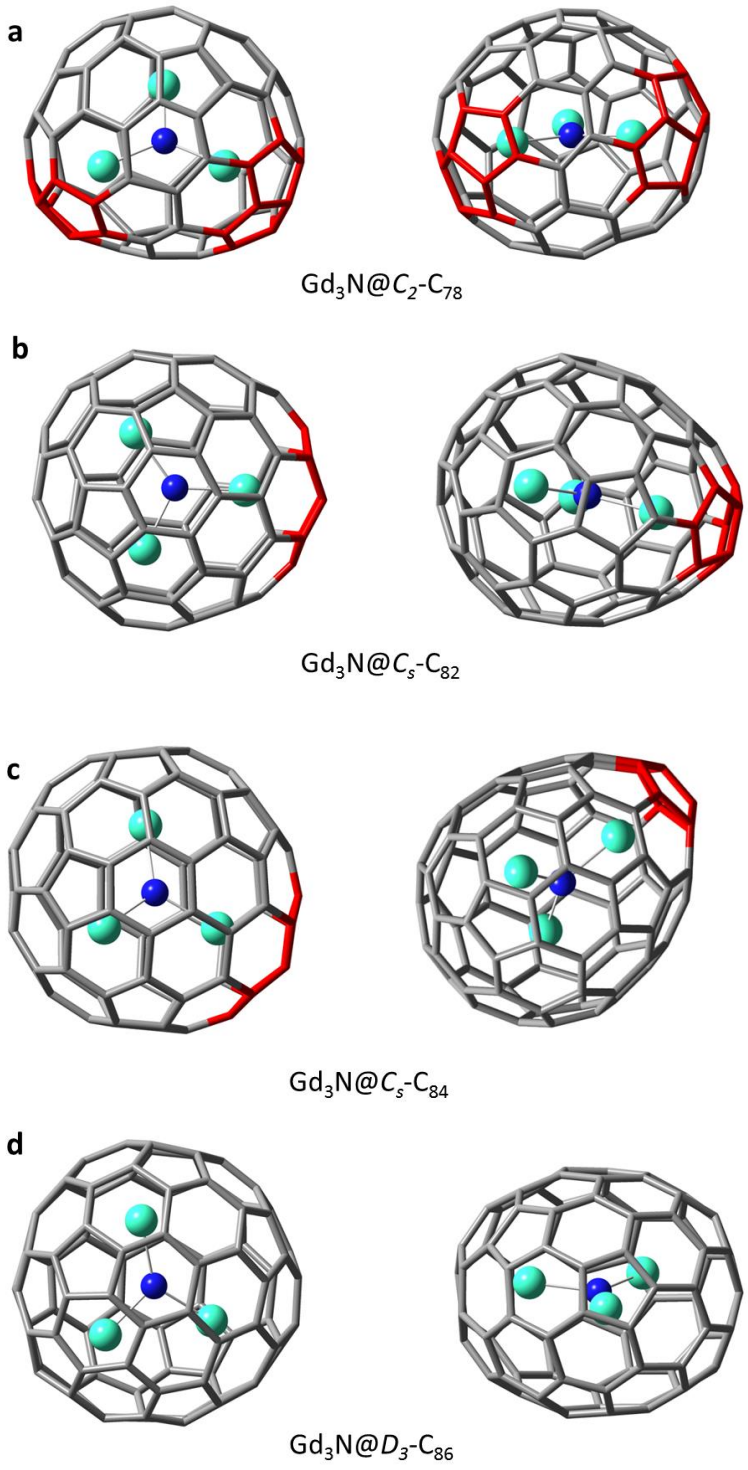

Figure 10. Minor gadolinium-based TNT EMFs that have been studied by the single crystal method. (a) $Gd_3N@C_2(22010)$-C_{78}. (b) $Gd_3N@C_s(39663)$-C_{82}. (c) $Gd_3N@C_s(51365)$-C_{84}. (d) $Gd_3N@D_3(19)$-C_{86}.

Metal carbide EMFs are another important family which have a metal-nonmetal cluster inside a fullerene cage. Balch et al. reported a family of gadolinium carbide metallofullerenes and determined the structure of $Gd_2C_2@D_3(85)$-C_{92}.[38] Very recently, Dorn, Balch and coworkers reported a low symmetry non-IPR gadolinium carbide EMF $Gd_2C_2@C_1(51383)$-C_{84}.[39]

Endohedral heterofullerenes are EMFs with heteroatoms replacing carbon atoms on the cage. In 2008, the first endohedral heterofullerenes, $Tb_2@C_{79}N$ and $Y_2@C_{79}N$ were reported by the Dorn group.[40] In 2011, the gadolinium version, $Gd_2@C_{79}N$, with 15/2 spin was reported by the same group.[41] Despite the paramagnetic nature of $Gd_2@C_{79}N$, it was shown that $Gd_2@C_{79}N$ was very stable at room temperature towards many radical scavengers, because the spin is buried inside the cage.

As the gadolinium based EMF family is under active research and quickly expanding, the application of the derivatives of these more exotic EMFs as MRI contrast agents has not been explored, leaving a very interesting topic in research on metallofullerenes.

1.3 Reference

(1) Popov, A. A.; Yang, S.; Dunsch, L.: Endohedral Fullerenes. *Chemical Reviews* **2013**.

(2) Heath, J. R.; O'Brien, S. C.; Zhang, Q.; Liu, Y.; Curl, R. F.; Tittel, F. K.; Smalley, R. E.: Lanthanum complexes of spheroidal carbon shells. *Journal of the American Chemical Society* **1985**, *107*, 7779-7780.

(3) Alvarez, M. M.; Gillan, E. G.; Holczer, K.; Kaner, R. B.; Min, K. S.; Whetten, R. L.: Lanthanum carbide (La_2C_{80}): a soluble dimetallofullerene. *The Journal of Physical Chemistry* **1991**, *95*, 10561-10563.

(4) Stevenson, S.; Rice, G.; Glass, T.; Harich, K.; Cromer, F.; Jordan, M. R.; Craft, J.; Hadju, E.; Bible, R.; Olmstead, M. M.; Maitra, K.; Fisher, A. J.; Balch, A. L.; Dorn, H. C.: Small-bandgap endohedral metallofullerenes in high yield and purity. *Nature* **1999**, *401*, 55-57.

(5) Wang, C. R.; Kai, T.; Tomiyama, T.; Yoshida, T.; Kobayashi, Y.; Nishibori, E.; Takata, M.; Sakata, M.; Shinohara, H.: Materials science - C_{66} fullerene encaging a scandium dimer. *Nature* **2000**, *408*, 426-427.

(6) Stevenson, S.; Mackey, M. A.; Stuart, M. A.; Phillips, J. P.; Easterling, M. L.; Chancellor, C. J.; Olmstead, M. M.; Balch, A. L.: A Distorted Tetrahedral Metal Oxide Cluster inside an Icosahedral Carbon Cage. Synthesis, Isolation, and Structural Characterization of $Sc_4(\mu_3\text{-}O)_2@I_h\text{-}C_{80}$. *Journal of the American Chemical Society* **2008**, *130*, 11844-11845.

(7) Dunsch, L.; Yang, S.; Zhang, L.; Svitova, A.; Oswald, S.; Popov, A. A.: Metal Sulfide in a C82 Fullerene Cage: A New Form of Endohedral Clusterfullerenes. *Journal of the American Chemical Society* **2010**, *132*, 5413-5421.

(8) Wang, T.-S.; Feng, L.; Wu, J.-Y.; Xu, W.; Xiang, J.-F.; Tan, K.; Ma, Y.-H.; Zheng, J.-P.; Jiang, L.; Lu, X.; Shu, C.-Y.; Wang, C.-R.: Planar Quinary Cluster inside a Fullerene Cage: Synthesis and Structural Characterizations of $Sc_3NC@C_{80}\text{-}I_h$. *Journal of the American Chemical Society* **2010**, *132*, 16362-16364.

(9) *http://www.fda.gov/NewsEvents/Newsroom/PressAnnouncements/2007/ucm108919.htm* **2007**.

(10) Mikawa, M.; Kato, H.; Okumura, M.; Narazaki, M.; Kanazawa, Y.; Miwa, N.; Shinohara, H.: Paramagnetic water-soluble metallofullerenes having the highest relaxivity for MRI contrast agents. *Bioconjugate Chemistry* **2001**, *12*, 510-514.

(11) Kato, H.; Kanazawa, Y.; Okumura, M.; Taninaka, A.; Yokawa, T.; Shinohara, H.: Lanthanoid Endohedral Metallofullerenols for MRI Contrast Agents. *Journal of the American Chemical Society* **2003**, *125*, 4391-4397.

(12) Bolskar, R. D.; Benedetto, A. F.; Husebo, L. O.; Price, R. E.; Jackson, E. F.; Wallace, S.; Wilson, L. J.; Alford, J. M.: First Soluble M@C_{60} Derivatives Provide Enhanced Access to Metallofullerenes and Permit in Vivo Evaluation of Gd@C_{60}[$C(COOH)_2$]$_{10}$ as a MRI Contrast Agent. *Journal of the American Chemical Society* **2003**, *125*, 5471-5478.

(13) Sitharaman, B.; Bolskar, R. D.; Rusakova, I.; Wilson, L. J.: Gd@C_{60}[$C(COOH)_2$]$_{10}$ and Gd@$C_{60}(OH)_x$: Nanoscale Aggregation Studies of Two Metallofullerene MRI Contrast Agents in Aqueous Solution. *Nano Letters* **2004**, *4*, 2373-2378.

(14) Tóth, É.; Bolskar, R. D.; Borel, A.; González, G.; Helm, L.; Merbach, A. E.; Sitharaman, B.; Wilson, L. J.: Water-Soluble Gadofullerenes: Toward High-Relaxivity, pH-Responsive MRI Contrast Agents. *Journal of the American Chemical Society* **2004**, *127*, 799-805.

(15) Zheng, J.-p.; Zhen, M.-M.; Ge, J.-C.; Liu, Q.-L.; Jiang, F.; Shu, C.-Y.; Alhadlaq, H. A.; Wang, C.-R.: Multifunctional gadofulleride nanoprobe for magnetic resonance imaging/fluorescent dual modality molecular imaging and free radical scavenging. *Carbon* **2013**, *65*, 175-180.

(16) Duchamp, J. C.; Demortier, A.; Fletcher, K. R.; Dorn, D.; Iezzi, E. B.; Glass, T.; Dorn, H. C.: An isomer of the endohedral metallofullerene $Sc_3N@C_{80}$ with D_{5h} symmetry. *Chemical Physics Letters* **2003**, *375*, 655-659.

(17) Olmstead, M. H.; de Bettencourt-Dias, A.; Duchamp, J. C.; Stevenson, S.; Marciu, D.; Dorn, H. C.; Balch, A. L.: Isolation and structural characterization of the endohedral fullerene $Sc_3N@C_{78}$. *Angewandte Chemie-International Edition* **2001**, *40*, 1223-+.

(18) Stevenson, S.; Fowler, P. W.; Heine, T.; Duchamp, J. C.; Rice, G.; Glass, T.; Harich, K.; Hajdu, E.; Bible, R.; Dorn, H. C.: Materials science - A stable non-classical metallofullerene family. *Nature* **2000**, *408*, 427-428.

(19) Kroto, H. W.: The stability of the fullerenes Cn, with n = 24, 28, 32, 36, 50, 60 and 70. *Nature* **1987**, *329*, 529-531.

(20) Dunsch, L.; Yang, S.: Metal nitride cluster fullerenes: Their current state and future prospects. *Small* **2007**, *3*, 1298-1320.

(21) Chaur, M. N.; Melin, F.; Ortiz, A. L.; Echegoyen, L.: Chemical, Electrochemical, and Structural Properties of Endohedral Metallofullerenes. *Angewandte Chemie-International Edition* **2009**, *48*, 7514-7538.

(22) Zhang, J.; Stevenson, S.; Dorn, H. C.: Trimetallic Nitride Template Endohedral Metallofullerenes: Discovery, Structural Characterization, Reactivity, and Applications. *Accounts of Chemical Research* **2013**.

(23) Stevenson, S.; Phillips, J. P.; Reid, J. E.; Olmstead, M. M.; Rath, S. P.; Balch, A. L.: Pyramidalization of Gd_3N inside a C_{80} cage. The synthesis and structure of $Gd_3N@C_{80}$. *Chemical Communications* **2004**, 2814-2815.

(24) Fatouros, P. P.; Corwin, F. D.; Chen, Z.-J.; Broaddus, W. C.; Tatum, J. L.; Kettenmann, B.; Ge, Z.; Gibson, H. W.; Russ, J. L.; Leonard, A. P.; Duchamp, J. C.; Dorn, H. C.: In vitro and in

vivo imaging studies of a new endohedral metallofullerene nanoparticle. *Radiology* **2006**, *240*, 756-764.

(25) Zhang, J.; Fatouros, P. P.; Shu, C.; Reid, J.; Owens, L. S.; Cai, T.; Gibson, H. W.; Long, G. L.; Corwin, F. D.; Chen, Z.-J.; Dorn, H. C.: High Relaxivity Trimetallic Nitride (Gd_3N) Metallofullerene MRI Contrast Agents with Optimized Functionality. *Bioconjugate Chemistry* **2010**, *21*, 610-615.

(26) Caravan, P.; Ellison, J. J.; McMurry, T. J.; Lauffer, R. B.: Gadolinium(III) Chelates as MRI Contrast Agents: Structure, Dynamics, and Applications. *Chemical Reviews* **1999**, *99*, 2293-2352.

(27) Shu, C.; Corwin, F. D.; Zhang, J.; Chen, Z.; Reid, J. E.; Sun, M.; Xu, W.; Sim, J. H.; Wang, C.; Fatouros, P. P.; Esker, A. R.; Gibson, H. W.; Dorn, H. C.: Facile Preparation of a New Gadofullerene-Based Magnetic Resonance Imaging Contrast Agent with High ^1H Relaxivity. *Bioconjugate Chemistry* **2009**, *20*, 1186-1193.

(28) Shultz, M. D.; Wilson, J. D.; Fuller, C. E.; Zhang, J.; Dorn, H. C.; Fatouros, P. P.: Metallofullerene-based Nanoplatform for Brain Tumor Brachytherapy and Longitudinal Imaging in a Murine Orthotopic Xenograft Model. *Radiology* **2011**, *261*, 136-143.

(29) Fillmore, H. L.; Shultz, M. D.; Henderson, S. C.; Cooper, P.; Broaddus, W. C.; Chen, Z. J.; Shu, C. Y.; Zhang, J. F.; Ge, J. C.; Dorn, H. C.; Corwin, F.; Hirsch, J. I.; Wilson, J.; Fatouros, P. P.: Conjugation of functionalized gadolinium metallofullerenes with IL-13 peptides for targeting and imaging glial tumors. *Nanomedicine* **2011**, *6*, 449-458.

(30) Fatouros, P. P.; Shultz, M. D.: Metallofullerenes: a new class of MRI agents and more? *Nanomedicine* **2013**, *8*, 1853-1864.

(31) Zhou, Z.: Liposome Formulation of Fullerene-Based Molecular Diagnostic and Therapeutic Agents. *Pharmaceutics* **2013**, *5*, 525-541.

(32) Zuo, T.; Walker, K.; Olmstead, M. M.; Melin, F.; Holloway, B. C.; Echegoyen, L.; Dorn, H. C.; Chaur, M. N.; Chancellor, C. J.; Beavers, C. M.; Balch, A. L.; Athans, A. J.: New egg-shaped fullerenes: non-isolated pentagon structures of $Tm_3N@C_s(51365)$-C_{84} and $Gd_3N@C_s(51365)$-C_{84}. *Chemical Communications* **2008**, 1067-1069.

(33) Beavers, C. M.; Zuo, T.; Duchamp, J. C.; Harich, K.; Dorn, H. C.; Olmstead, M. M.; Balch, A. L.: $Tb_3N@C_{84}$: An improbable, egg-shaped endohedral fullerene that violates the isolated pentagon rule. *Journal of the American Chemical Society* **2006**, *128*, 11352-11353.

(34) Mercado, B. Q.; Beavers, C. M.; Olmstead, M. M.; Chaur, M. N.; Walker, K.; Holloway, B. C.; Echegoyen, L.; Balch, A. L.: Is the isolated pentagon rule merely a suggestion for endohedral fullerenes? The structure of a second egg-shaped endohedral fullerene-$Gd_3N@C_s(39663)$-C_{82}. *Journal of the American Chemical Society* **2008**, *130*, 7854-7855.

(35) Beavers, C. M.; Chaur, M. N.; Olmstead, M. M.; Echegoyen, L.; Balch, A. L.: Large Metal Ions in a Relatively Small Fullerene Cage: The Structure of $Gd_3N@C_2(22010)$-C_{78} Departs from the Isolated Pentagon Rule. *Journal of the American Chemical Society* **2009**, *131*, 11519-11524.

(36) Chaur, M. N.; Aparicio-Angles, X.; Mercado, B. Q.; Elliott, B.; Rodriguez-Fortea, A.; Clotet, A.; Olmstead, M. M.; Balch, A. L.; Poblet, J. M.; Echegoyen, L.: Structural and Electrochemical Property Correlations of Metallic Nitride Endohedral Metallofullerenes. *Journal of Physical Chemistry C* **2010**, *114*, 13003-13009.

(37) Zhang, J.; Bearden, D. W.; Fuhrer, T.; Xu, L.; Fu, W.; Zuo, T.; Dorn, H. C.: Enhanced Dipole Moments in Trimetallic Nitride Template Endohedral Metallofullerenes with the Pentalene Motif. *Journal of the American Chemical Society* **2013**, *135*, 3351-3354.

(38) Yang, H.; Lu, C.; Liu, Z.; Jin, H.; Che, Y.; Olmstead, M. M.; Balch, A. L.: Detection of a Family of Gadolinium-Containing Endohedral Fullerenes and the Isolation and Crystallographic Characterization of One Member as a Metal-Carbide Encapsulated inside a Large Fullerene Cage. *Journal of the American Chemical Society* **2008**, *130*, 17296-17300.

(39) Zhang, J.; Bowles, F. L.; Bearden, D. W.; Ray, W. K.; Fuhrer, T.; Ye, Y.; Dixon, C.; Harich, K.; Helm, R. F.; Olmstead, M. M.; Balch, A. L.; Dorn, H. C.: A missing link in the transformation from asymmetric to symmetric metallofullerene cages implies a top-down fullerene formation mechanism. *Nature Chemistry* **2013**, *5*, 880-885.

(40) Zuo, T.; Xu, L.; Beavers, C. M.; Olmstead, M. M.; Fu, W.; Crawford, T. D.; Balch, A. L.; Dorn, H. C.: $M_2@C_{79}N$ (M = Y, Tb): Isolation and Characterization of Stable Endohedral Metallofullerenes Exhibiting M-M Bonding Interactions inside Aza[80]fullerene Cages. *Journal of the American Chemical Society* **2008**, *130*, 12992-12997.

(41) Fu, W.; Zhang, J.; Fuhrer, T.; Champion, H.; Furukawa, K.; Kato, T.; Mahaney, J. E.; Burke, B. G.; Williams, K. A.; Walker, K.; Dixon, C.; Ge, J.; Shu, C.; Harich, K.; Dorn, H. C.: $Gd_2@C_{79}N$: Isolation, Characterization, and Monoadduct Formation of a Very Stable Heterofullerene with a Magnetic Spin State of S=15/2. *Journal of the American Chemical Society* **2011**, *133*, 9741-9750.

Chapter 2 Synthesis and Characterization and Magnetic Resonance Imaging Study of $Gd_3N@C_{80}$ and $Gd_3N@C_{84}$ Metallofullerenols: The Importance of Cage Symmetry on Relaxivity

This Chapter is adopted with modification from extensively collaborative work which is described in an accepted manuscript to be published in the *Journal of the American Chemical Society* (DOI: 10.1021/ja412254k) "$Gd_3N@C_{84}(OH)_x$: A New Egg-Shaped Metallofullerene Magnetic Resonance Imaging Contrast Agent" by Jianyuan Zhang, Youqing Ye, Ying Chen, Christopher Pregot, Tinghui Li, Sharavanan Balasubramaniam, David B. Hobart, Yafen Zhang, Sungsool Wi, Richey M. Davis, Louis A. Madsen , John R. Morris, Stephen M. LaConte, Gordon T. Yee and Harry C. Dorn. In the original manuscript, J. Z. and C. P. performed sample purification (not included in this chapter); J. Z. and G. T. Y. performed magnetization measurements (not included in this chapter); J. Z., Y. C. and S. W. obtained NMR data for the functionalized $Y_3N@C_{80}$ (not included in this chapter); J. Z. and Y. Y. performed metallofullerene functionalization and product purification **(2.2.1)**; J. Z. and Y. Y. obtained Gd concentration data **(2.2.2)**; Y. Y., Y. C. and T. L. obtained relaxivity data using the instrument in the Madsen laboratory **(2.2.3 and 2.5)**; J. Z. obtained UV-vis-NIR data **(2.3)**; Y. Y., Y. Z. and D. B. H. obtained IR and XPS data using the instrument in the Morris laboratory **(2.3)**; J. Z., S. B. and Y. Y. obtained DLS data using the instrument in the Davis laboratory **(2.4)**; J. Z. and Y. Y. prepared the samples for MR imaging performed by S. M. L. and H. C. D. using the instrument in the LaConte laboratory **(2.6)**. J. Z. and Y. Y. analyzed the data and produced the figures; H. C. D. finalized the manuscript.

2.1 Introduction

Gadolinium ions are widely used in magnetic resonance imaging (MRI) contrast agents for their paramagnetic property and long spin-lattice relaxation time.[1] Gadolinium based endohedral metallofullerenes (EMFs) are considered promising for next generation contrast agents for higher safety and better efficiency. Early research on water-soluble derivatives of gadolinium metallofullerenes ("gadofullerenes") was pioneered by the Shinohara[2,3] and Wilson[4-6] groups and focused on mono-metal gadofullerenes, namely, $Gd@C_{82}$ and $Gd@C_{60}$. More recently, attention

has focused on the trimetallic nitride template (TNT) endohedral metallofullerenes,[7,8] and many water-soluble derivatives of $Gd_3N@I_h$-C_{80} and Gd-containing mixed metal TNT EMFs have been synthesized and tested as MRI contrast agents.[9-15] One distinct advantage of the TNT EMF derivatives is their high synthetic yield and up to three (as opposed to one) Gd^{3+} ions inside a single fullerene cage.

Currently the research on TNT EMF based contrast agents is limited to I_h-C_{80} cage derivatives, even though other TNT EMF members have very different symmetry and shape[8] that may affect their relaxation behavior. For example, the pentalene-containing $Gd_3N@C_s$(51365)-C_{84} (referred as "$Gd_3N@C_{84}$" in the rest of this chapter since it is the only reported Gd_3NC_{84} isomer) has an elipsodal egg-shape,[16] in direct contrast to spherical $Gd_3N@I_h$-C_{80}[17] (Figure 1). Several other important structural features are very different between the two TNT EMFs. First, $Gd_3N@I_h$-C_{80} has a pyramidal Gd_3N cluster, whereas $Gd_3N@C_{84}$ has a planar cluster. Second, based on the results in a corresponding ^{89}Y NMR study of diamagnetic $Y_3N@I_h$-C_{80} and $Y_3N@C_s$(51365)-C_{84},[18] $Gd_3N@I_h$-C_{80} should exhibit isotropic motion of the $(Gd_3N)^{6+}$ cluster, whereas, $Gd_3N@C_{84}$ should exhibit restricted motion because of stronger association of one Gd atom to the pentalene motif. Third, the strong Gd-pentalene interaction provides a significantly enhanced dipole moment for $Gd_3N@C_{84}$.[19] All of these differences may lead to different properties of their derivatives that could significantly alter MRI contrast efficiencies. In this chapter I present a study on $Gd_3N@C_{84}$[16] and the corresponding water soluble functionalized $Gd_3N@C_{84}(OH)_x$ directly compared with the $Gd_3N@C_{80}$ counterpart as a potential new MRI contrast agent.

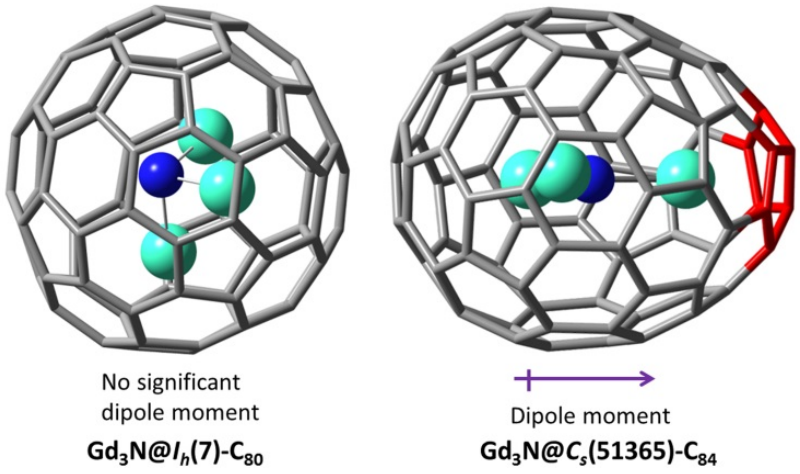

Figure 1. Structures of $Gd_3N@I_h(7)$-C_{80} (left) and $Gd_3N@C_s(51365)$-C_{84} (right, pentalene unit shown in red).

2.2 Experimental section

2.2.1 Synthesis of the Gd metallofullerenols

The starting materials, namely, $Gd_3N@C_{80}$ and $Gd_3N@C_{84}$, were purified by our group members Jianyuan Zhang and Christopher Pregot following a reported procedure.[20] Before functionalization, the purity of the samples was checked by HPLC and mass spectrometry (Figure 2). In both cases, the mass spectrometry showed a single sharp peak corresponding to the right molecular weight (1445 for $Gd_3N@C_{80}$, 1493 for $Gd_3N@C_{84}$), and the HPLC showed a single, symmetric peak that suggests isomeric purity.

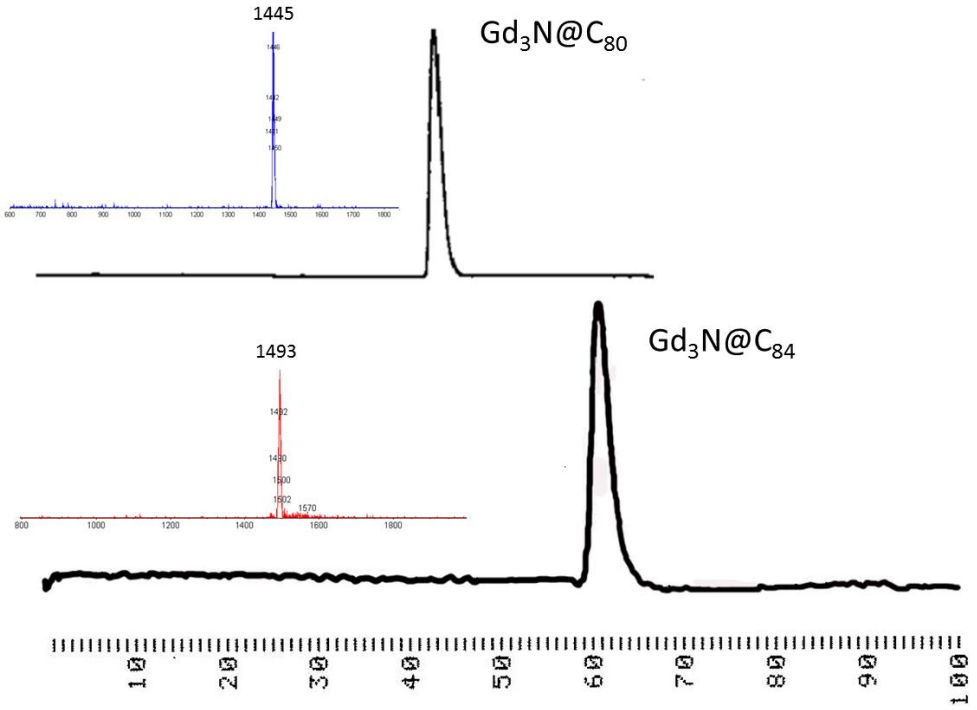

Figure 2. HPLC traces of purified $Gd_3N@C_{80}$ (top) and $Gd_3N@C_{84}$ (bottom) on a 5PYE column (0.5 inch diameter), with toluene as eluent at 2 mL/min. Insets: LD-TOF mass-spectrometry of the purified $Gd_3N@C_{80}$ and $Gd_3N@C_{84}$.

The functionalization of a Gd TNT EMFs (Figure 3) was performed with the help of Jianyuan Zhang following the procedure reported by Shinohara et al.[2] Briefly, to toluene solutions containing $Gd_3N@C_{80}$ (~1.0 mg) and $Gd_3N@C_{84}$ (~0.6 mg) respectively, were added 2 mL of 50 wt% NaOH solution and 2 drops of tetrabutyl ammonium hydroxide and stirred at room temperature for 15 minutes. After the precipitation of a brown sludge, the toluene was removed by careful decantation. Then 10 mL more water was added to each reaction flask and the resulting mixtures were stirred overnight to give light brown aqueous solutions. Dilute hydrochloric acid was added dropwise to adjust the pH of the solutions to neutral. Then the solutions were placed in a cellulose dialysis bag (MWCO=500) for a 7-day dialysis (water changed every 24 hours) to give the water solutions of the corresponding hydroxylated Gd TNT

EMFs, or Gd metallofullerenols. As shown in Figure 3, although the reaction aims to introduce hydroxyl groups, some carbonyl groups can be generated on the cage due to isomerization.

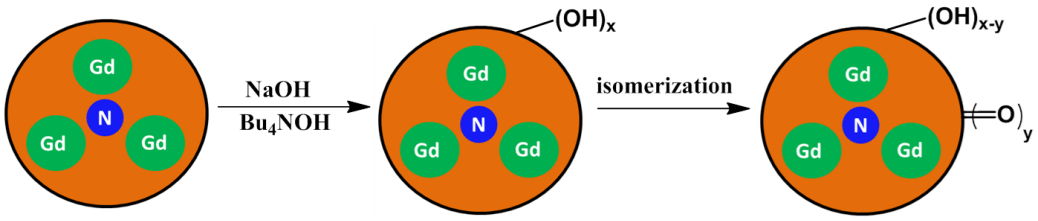

Figure 3. Functionalization scheme for the gadolinium based TNT EMFs.

2.2.2 Concentration measurement of the functionalized TNT EMFs

The concentration of the water soluble TNT EMF derivatives was measured with the help of Jianyuan Zhang at Virginia Commonwealth University (VCU) by the inductively coupled plasma mass spectroscopy (ICP-MS) method after dilution in 2% nitric acid solution. In each reaction, the Gd TNT EMF is the only source of the gadolinium ions and the fullerene cages are not broken during the functionalization process. Therefore, the measured Gd^{3+} concentration divided by three gives the concentration of the Gd TNT EMF.

2.2.3 Relaxivity measurements of the functionalized TNT EMFs

NMR relaxation measurements were performed on Bruker Minispec mq20 (0.47 T) and mq60 (1.41 T) analyzers as well as a Bruker Avance III 400 MHz (9.4 T) wide bore spectrometer equipped with a MIC 400 W1/S2 probe and 5 mm ^{1}H coil. The measurements on the 9.4 T instrument were performed by Ying Chen from the Department of Chemistry at Virginia Tech. The spin-lattice relaxation time T_1 was measured by the inversion-recovery method. The spin-spin relaxation time T_2 was measured using an incremented echo-train CPMG pulse sequence. Errors in T_1 and T_2 values are generally less than ± 2%. All samples were placed in a 5 mm NMR tube for the measurements. The concentration range for $Gd_3N@C_{80}$ metallofullerenols

was 0.51-2.5 μM, and the concentration range for $Gd_3N@C_{84}$ metallofullerenols was 0.28-1.4 μM.

2.3 Structural characterization of the functionalized TNT EMFs

$Gd_3N@C_{80}$ and $Gd_3N@C_{84}$ were converted to the corresponding metallofullerenols with the procedure described above.[2] The UV-vis-NIR data of $Gd_3N@C_{80}$ metallofullerenol and $Gd_3N@C_{84}$ metallofullerenol were obtained by Jianyuan Zhang. The spectra exhibit decreased conjugation features in comparison with the corresponding parent EMFs (Figure. 4), confirming the loss of extended aromaticity.

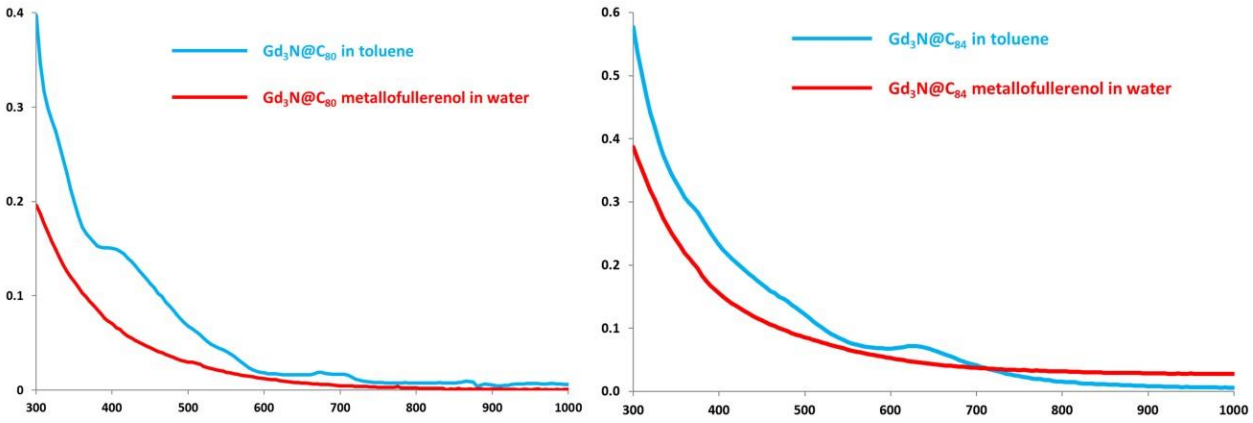

Figure 4. UV-vis-NIR spectra of Gd metallofullerenes (blue) and their metallofullerenols (red). Left: UV-vis-NIR spectrum of $Gd_3N@C_{80}$ and its metallofullerenol. Right: UV-vis-NIR spectrum of $Gd_3N@C_{84}$ and its metallofullerenol.

Although the reaction was intended to introduce hydroxyl groups, the existence of carbonyl groups resulting from rearrangements was confirmed by the FT-IR (Figure 5) and XPS (Figure 6) spectra of the $Gd_3N@C_{80}$ and $Gd_3N@C_{84}$ metallofullerenols. The FT-IR data were obtained with the help of Yafen Zhang from the Department of Chemistry at Virginia Tech. In the spectra of $Gd_3N@C_{80}$ and $Gd_3N@C_{84}$ metallofullerenols (Figure 5), the carbonyl content is reflected by

the intensity of the C=O peaks around 1700 cm^{-1}, as well as the C-H peaks at 2880-3000 cm^{-1} associated with the keto-enol type isomerization, and the intensity of these peaks suggest the $Gd_3N@C_{84}$ metallofullerenol has a lower carbonyl content.

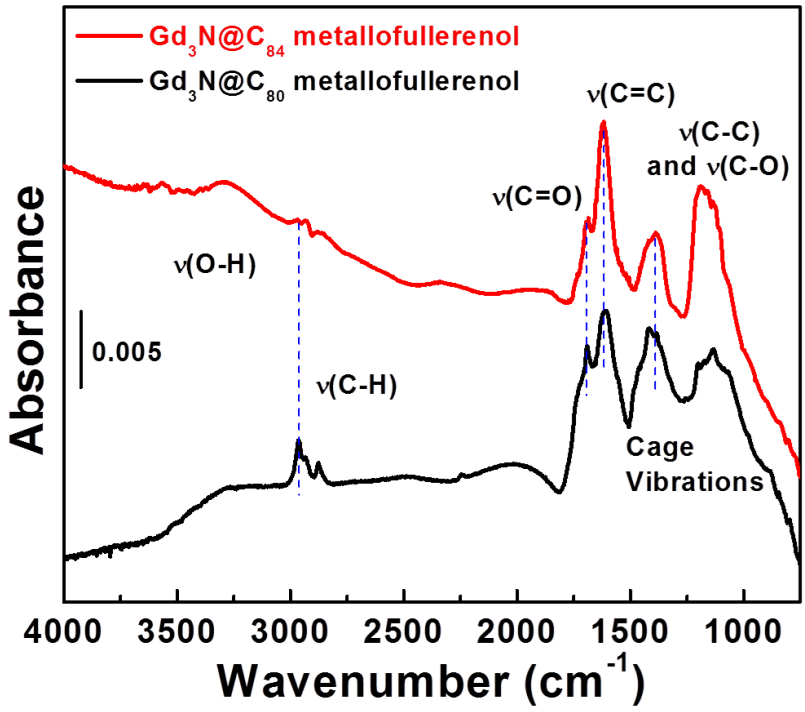

Figure 5. FT-IR spectra for the $Gd_3N@C_{80}$ and $Gd_3N@C_{84}$ metallofullerenols.

Furthermore, XPS is a well-established method to investigate the composition of fullerenols.[11,21-23] XPS data for $Gd_3N@C_{80}$ and $Gd_3N@C_{84}$ fullerenols were obtained with the help of David B. Hobart from the Department of Chemistry at Virginia Tech. The data were fitted using three peaks (Fig. 4d, e): the C-C bond (284.5 eV), the C-O single bond (285.7 eV) and the C=O double bond (288.3 eV). In both cases about 40% of the carbon atoms were functionalized with oxygen; however, consistent with the FT-IR results, a clear difference was shown for the carbonyl content. The estimated formula for $Gd_3N@C_{80}$ metallofullerenol was $Gd_3N@C_{80}O_{11}(OH)_{21}$, and that for $Gd_3N@C_{84}$ metallofullerenol was $Gd_3N@C_{84}O_6(OH)_{28}$.

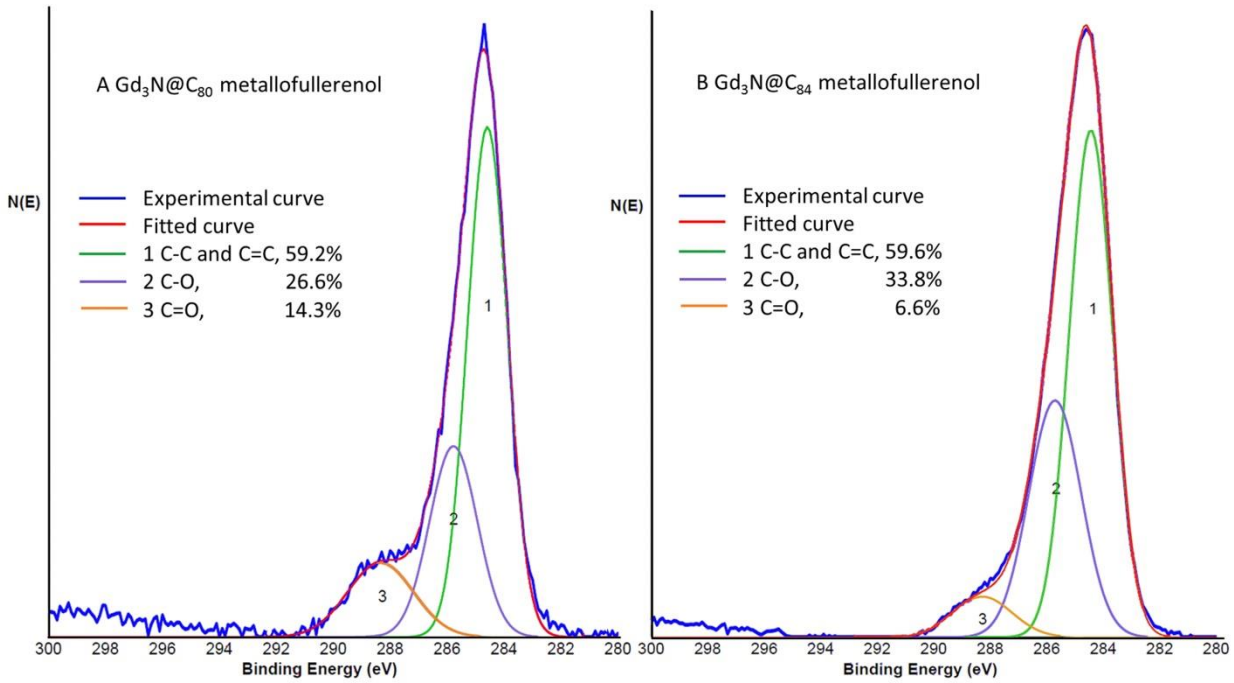

Figure 6. XPS for the $Gd_3N@C_{80}$ metallofullerenol and $Gd_3N@C_{84}$ metallofullerenol.

In addition, the element survey and the N1s spectra in XPS also confirmed that gadolinium and nitrogen elements were contained in the samples (Figure 7).

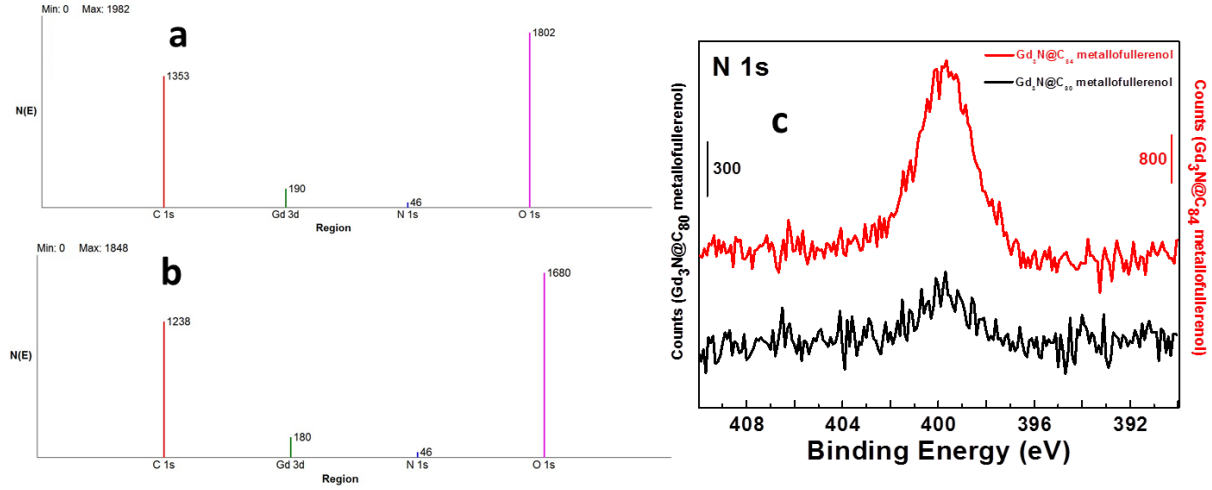

Figure 7. XPS element survey and N1s spectra. (a) Element survey for $Gd_3N@C_{80}$ metallofullerenol. (b) Element survey for $Gd_3N@C_{80}$ metallofullerenol. (c) Superimposed XPS N1s spectra for $Gd_3N@C_{80}$ metallofullerenol (black) and $Gd_3N@C_{84}$ metallofullerenol (red).

2.4 Dynamic light scattering study of the metallofullerenol aggregates

Water-soluble metallofullerene derivatives form aggregates in water, the size of which has a decisive role in their relaxivity.[24] Dynamic light scattering experiments were performed by Jianyuan Zhang, Youqing Ye and Sharavanan Balasubramaniam using the instrument in the Davis laboratory to investigate the hydrodynamic size of the aggregates formed by the trimetallic nitride metallofullerenols. The concentrations of both solutions (colloids) were estimated to be 70 μM. The results represent the average of 3 reproducible runs, and are shown in Figure 8. Each metallofullerenol had two different stages of aggregation. The $Gd_3N@I_h$-C_{80} metallofullerenol showed two unresolved peaks (seen as one asymmetric peak) with a mean radius of 125 nm (~2 million molecules), which is similar to the carboxylated and hydroxlated derivative[11] and short-PEG chain derivative[13] of $Gd_3N@I_h$-C_{80}. Meanwhile, the $Gd_3N@C_{84}$ metallofullerenol showed a well-resolved bimodal distribution. A small peak was centered at 9.5 nm (~1,000 molecules), while the large peak showed a mean radius of 179 nm (~5-6 million molecules), which is considerably larger than the counterpart aggregates of metallofullerenol $Gd_3N@I_h$-C_{80}. The separate two stages of aggregation for hydroxylated $Gd_3N@C_{84}$ highly resemble the cases of poly(ethylene glycol) (PEG) functionalized $Gd_3N@C_{80}$,[13] in which longer PEG chains led to higher amounts of small aggregates due to steric hindrance. For $Gd_3N@C_{84}$, the egg-shaped cage plus certain functionalization site in some molecules may generate larger steric hindrance which prevents some aggregates to pack larger. Therefore, the resolved peak for lower aggregate could be related to the less spherical shape of $Gd_3N@C_{84}$.

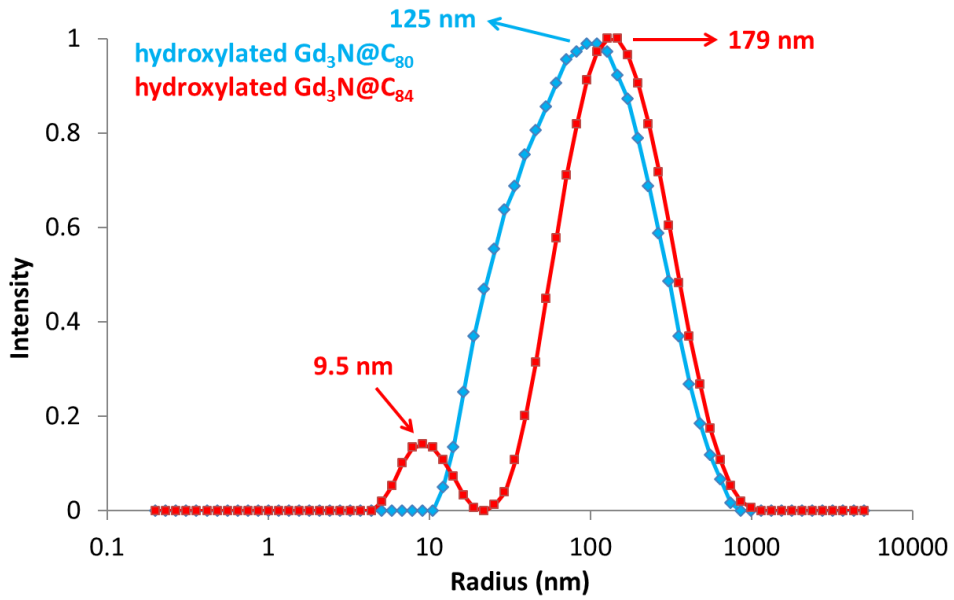

Figure 8. Hydrodynamic size distribution of metallofullerenol derivatives of $Gd_3N@I_h$-C_{80} and $Gd_3N@C_{84}$.

2.5 Relaxivity of the trimetallic nitride metallofullerenols

The ability of contrast agents to enhance MRI contrast is evaluated by relaxivity, which is defined by the equation:

$$\frac{1}{T_{i,\ obs}} = \frac{1}{T_{i,\ H_2O}} + \frac{1}{T_{i,\ para}} = \frac{1}{T_{i,\ H_2O}} + r_i[M] \quad i = 1, 2$$

where T_1 and T_2 are longitudinal and transverse relaxation time, respectively. The relaxation rate (reciprocal of relaxation time) is determined by both diamagnetic (water) and paramagnetic (contrast agent) species, and the ratio of paramagnetic relaxation rate to the concentration is the relaxivity of the paramagnetic compound, which can be experimentally obtained by the slope of ($1/T_i$) vs. concentration of the paramagnetic contrast agents.

The relaxivity values of $Gd_3N@C_{80}$ metallofullerenol and $Gd_3N@C_{84}$ metallofullerenol were obtained at 0.47 T, 1.4 T and 9.4 T magnetic field, respectively, and the results are shown in

Figures 9-11. The results and the r_2/r_1 values are summarized in Table 1. Compared to the ~4-6 $mM^{-1}S^{-1}$ relaxivity for the commercial contrast agent Gd-DTPA (Magnivest®), the relaxivity values for the trimetallic nitride metallofullerenols are significantly higher, and they did not change meaningfully from low to mid-field strength, but significantly decreased at high field. The $Gd_3N@C_{84}$ metallofullerenol has considerably higher relaxivity values than $Gd_3N@C_{80}$ metallofullerenol, suggesting that $Gd_3N@C_{84}$ is an excellent candidate as a new MRI contrast agent if it can be produced in large quantities.

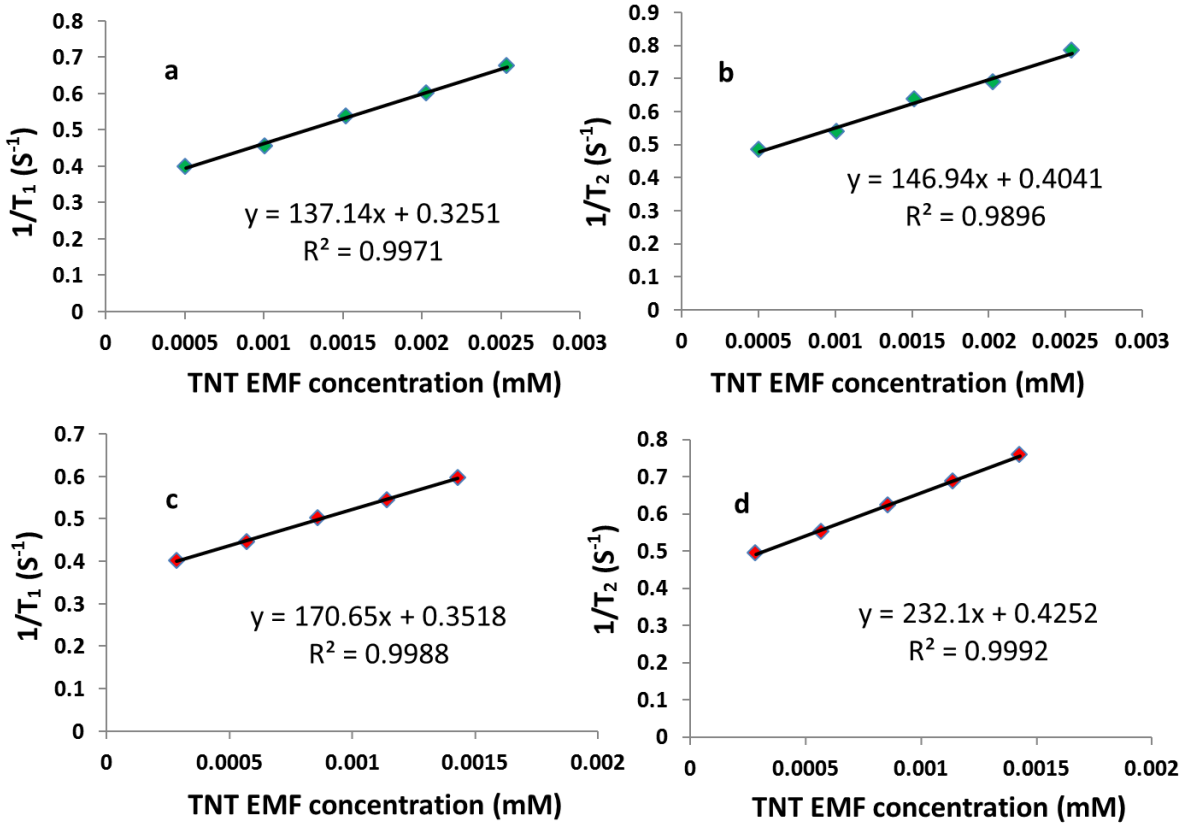

Figure 9. T_1 and T_2 measurements on a 20 MHz (0.47 T) instrument. (a) T_1 results for functionalized $Gd_3N@C_{80}$. (b) T_2 results for functionalized $Gd_3N@C_{80}$. (c) T_1 results for functionalized $Gd_3N@C_{84}$. (d) T_2 results for functionalized $Gd_3N@C_{84}$.

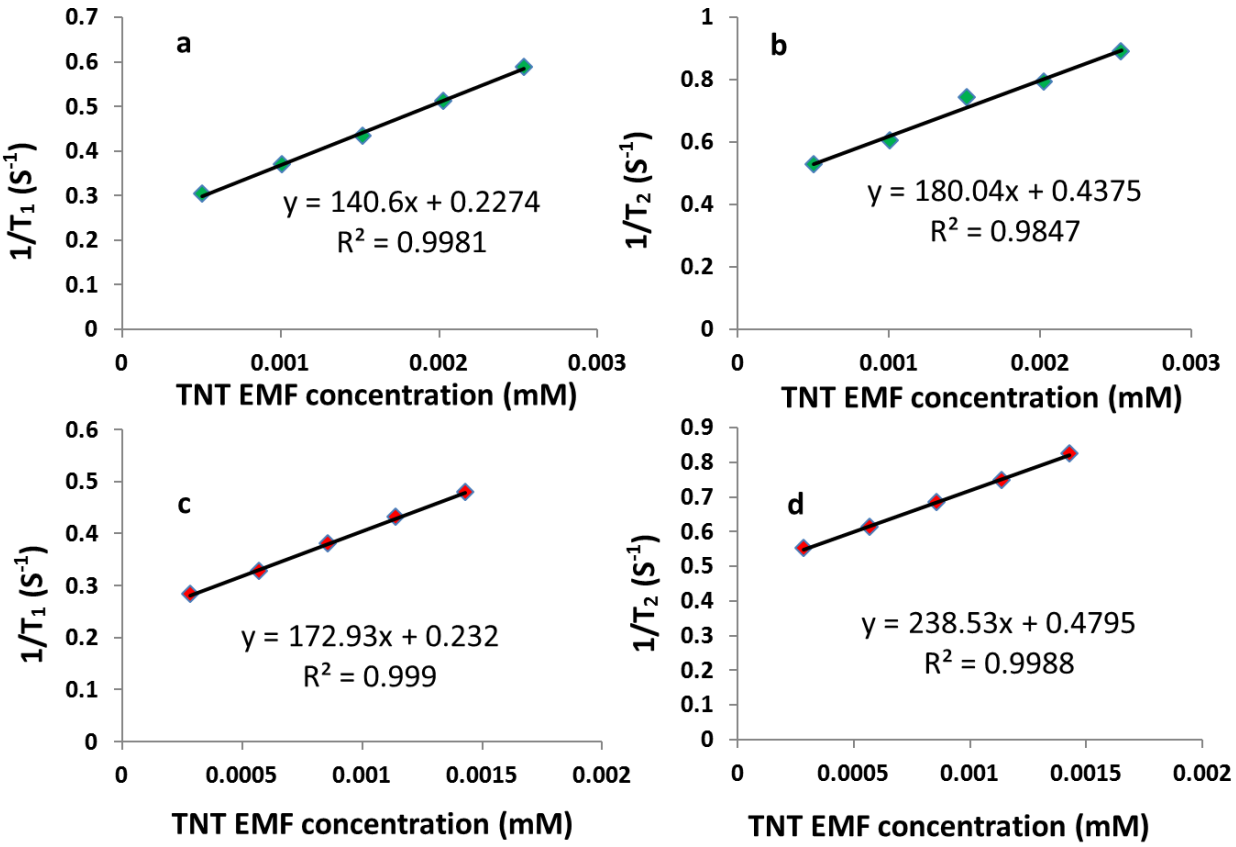

Figure 10. T_1 and T_2 measurements on a 60 MHz (1.4 T) instrument. (a) T_1 results for functionalized $Gd_3N@C_{80}$. (b) T_2 results for functionalized $Gd_3N@C_{80}$. (c) T_1 results for functionalized $Gd_3N@C_{84}$. (d) T_2 results for functionalized $Gd_3N@C_{84}$.

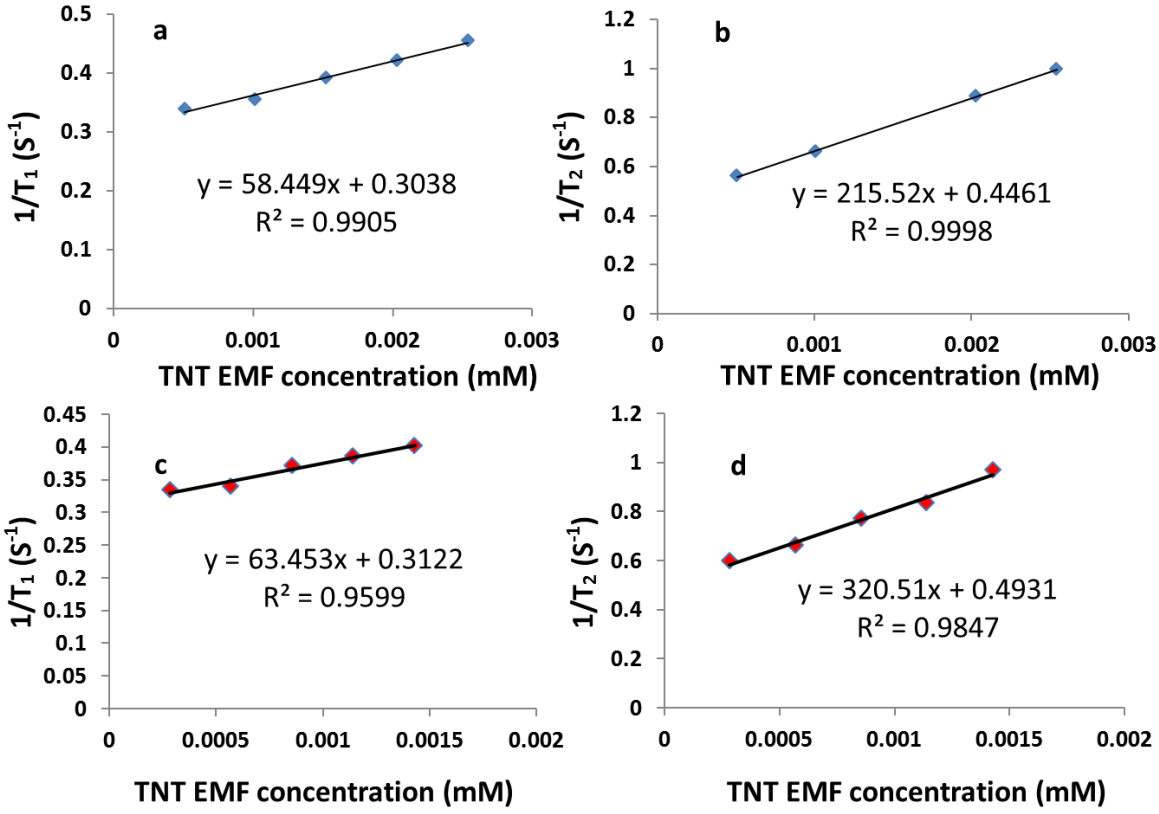

Figure 11. T_1 and T_2 measurements on a 400 MHz (9.4 T) instrument. (a) T_1 results for functionalized $Gd_3N@C_{80}$. (b) T_2 results for functionalized $Gd_3N@C_{80}$. Note that one data point was abandoned due to an accidental crack of the NMR tube which caused unreasonable result. (c) T_1 results for functionalized $Gd_3N@C_{84}$. (d) T_2 results for functionalized $Gd_3N@C_{84}$.

Table 1. Relaxivity values for the $Gd_3N@C_{80}$ and $Gd_3N@C_{84}$ metallofullerenols. For all relaxivity values, the units are $mM^{-1}S^{-1}$.

Metallofullerenol	0.47 T			1.4 T			9.4 T		
	r_1	r_2	r_2/r_1	r_1	r_2	r_2/r_1	r_1	r_2	r_2/r_1
$Gd_3N@C_{80}O_{11}(OH)_{21}$	137	146	1.07	140	180	1.28	58	215	3.7
$Gd_3N@C_{84}O_6(OH)_{28}$	170	232	1.36	173	238	1.38	63	320	5.1

2.6 *In vitro* MRI study of trimetallic nitride metallofullerenols

For a visual confirmation of the efficiency of the trimetallic nitride metallofullerenols as contrast agents and a direct comparison between $Gd_3N@C_{80}$ and $Gd_3N@C_{84}$ metallofullerenols, T_1-weighted MR imaging was performed for their solutions in comparison with the commercial agent Omniscan (Fig. 12). The images were obtained by Stephen M. LaConte and Harry C. Dorn in the LaConte laboratory at VTCRI using the samples prepared by Jianyuan Zhang and Youqing Ye. Significant signal enhancements were observed for both metallofullerenols in a concentration range of 0.3-3 μM (based on the metallofullerenol molecule). The r_1 signal intensity (brightness) of the 0.51 μM $Gd_3N@C_{80}$ (Fig. 12a) metallofullerenol versus the 0.28 μM $Gd_3N@C_{84}$ metallofullerenol (Fig. 12e) are qualitatively comparable, but are in 50-100 fold lower concentrations than needed for comparable contrast with Omniscan (24.2 μM) (Figure. 12d,h). In each respective column of Figure. 12, the $Gd_3N@C_{80}$ metallofullerenols (Figure. 6 a-c) have 1.8 fold higher concentrations compared to $Gd_3N@C_{84}$ metallofullerenols (Figure. 6 e-g), but still provide marginally lower contrast. In Figure 12b and 12g the metallofullerenols have similar concentration, but the image for $Gd_3N@C_{84}$ metallofullerenol is much brighter. These direct comparisons suggest that the $Gd_3N@C_{84}$ metallofullerenol prepared in this study is somewhat more effective as a contrast agent than $Gd_3N@C_{80}$ metallofullerenol in qualitative T_1-weighted MR imaging at clinical scanner magnetic field strengths.

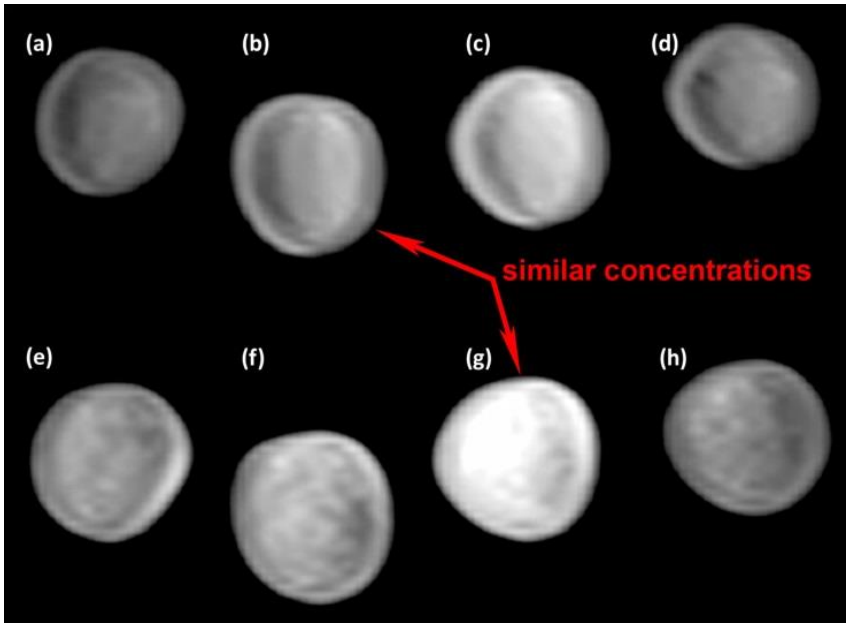

Figure 12. T_1 weighted MR imaging at 3 T (123 MHz) with Gd metallofullerenols as contrast agents. Top line from left to right: (a) 0.51 μM $Gd_3N@C_{80}$ metallofullerenol, (b) 1.5 μM $Gd_3N@C_{80}$ metallofullerenol, (c) 2.5 μM $Gd_3N@C_{80}$ metallofullerenol, (d) 24.2 μM omniscan. Bottom line from left to right: (e) 0.28 μM $Gd_3N@C_{84}$ metallofullerenol, (f) 0.86 μM $Gd_3N@C_{84}$ metallofullerenol, (g) 1.4 μM $Gd_3N@C_{84}$ metallofullerenol, (h) 24.2 μM omniscan.

2.7 **Discussion**

2.7.1 Comparison of the relaxivities of monometallic EMF and TNT EMF metallofullerenol

The magnetic moment and proton relaxivity values are directly related. For T_1 weighted MRI, the contrast of the image can be represented by $1/T_1$, which is driven by dipole-dipole interactions and scalar contact (SC) interactions:

$$\frac{1}{T_1} = \frac{1}{T_1^{DD}} + \frac{1}{T_1^{SC}}$$

The two terms are determined by the equations below:[1]

$$\frac{1}{T_1^{DD}} = \frac{2}{15}\frac{\gamma_1^2 g^2 \mu_B^2 s(s+1)}{r^6}\left[\frac{3\tau_{c1}}{(1+\omega_I^2 3\tau_{c1}^2)} + \frac{7\tau_{c2}^2}{(1+\omega_S^2\tau_{c2}^2)}\right]$$

$$\frac{1}{T_1^{SC}} = \frac{2}{3}s(s+1)\left(\frac{A}{\hbar}\right)^2\left[\frac{\tau_e^2}{(1+\omega_S^2\tau_{e2}^2)}\right]$$

In the case of gadolinium EMFs, the dipole-dipole term is the dominant factor. Therefore, it is easily derived that

$$\mu_{eff}{}^2 \propto \frac{1}{T_1^{DD}}$$

The paramagnetism (effective magnetic moment) of the gadofullerenes originates from the 7 unpaired *f* electrons of the Gd^{3+}, and the functionalization only relates to the *s* and *p* orbitals of the carbon atoms on the fullerene cage. If this functionalization does not significantly change the effective magnetic moment of the encapsulated cluster (Gd_3N), the r_1 of the metallofullerenol should be proportional to the square of the μ_{eff} of the corresponding parent gadofullerene. The μ_{eff} of $Gd@C_{82}$ was previously determined to be 6.90 μ_B.[25,26] In a study performed by Jianyuan Zhang our group, the μ_{eff} of $Gd_3N@C_{80}$ and $Gd_3N@C_{84}$ are 10.8 μ_B and 11.5 μ_B, respectively. Therefore, the metallofullerenols in current work should have ~2-3 fold higher r_1 compared to the same type metallofullerenol, $Gd@C_{82}$.

Experimental r_1 values for gadofullerene derivatives $Gd@C_{82}$, $Gd_3N@C_{80}$, and $Gd_3N@C_{84}$ both from the literature[2,11-13] and current work are shown in Figure 12 and Table 2. As a semi-quantitative overall trend, at respective field strengths, the $Gd_3N@C_{80}$ derivative has r_1 values of 1.8-2.0 fold higher than the r_1 of $Gd@C_{82}$ metallofullerenol for the same functionalization. However, the $Gd_3N@C_{84}$ metallofullerenol has 2.0-2.4 fold higher values in comparison with the $Gd@C_{82}$ for the same functionalization used in the present study. Furthermore, a comparison of the r_1 values for the $Gd@C_{82}$, $Gd_3N@C_{80}$, and $Gd_3N@C_{84}$ derivatives versus other Gd TNT

EMFs with different functionalization illustrate a factor of ~2-3 higher relaxivity relative to $Gd@C_{82}$ at all magnetic field strengths, which is consistent with what is expected from the molecular magnetic moments.

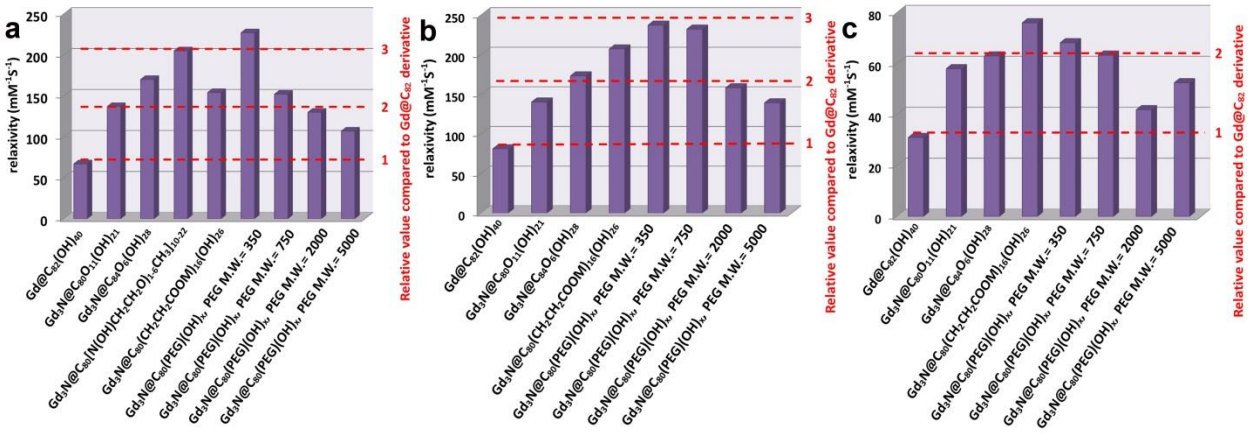

Figure 13. Summary of r_1 relaxivity values for $Gd@C_{82}$, $Gd_3N@C_{80}$, and $Gd_3N@C_{84}$ derivatives at (a) low magnetic field (0.35-0.47 T), (b) medium magnetic field (1.0-2.4 T) and (c) high magnetic field (4.7 T). In each panel, the left three columns represent the metallofullerene derivatives functionalized in the procedure described in current study. The data from previous reports cited in this figure are from refs 2, 11, 12 and 13.

Table 2. T_1 relaxivity of $Gd_3N@C_{80}$ and $Gd_3N@C_{84}$ derivatives compared to $Gd@C_{82}$ metallofullerenol.

Gadofullerene derivative	Magnetic Field	r_1 ($mM^{-1}S^{-1}$)	Relative to $Gd@C_{82}(OH)_{40}$
$Gd@C_{82}(OH)_{40}$	0.47 T	67	1 (for low-field)
	1.0 T	81	1 (for mid-field)
	4.7 T	31	1 (for high-field)
$Gd_3N@C_{80}(CH_2CH_2COOM)_{16}(OH)_{26}$ (M=H, Na) [11]	0.35 T	154	2.3 (compared to low-field)
	2.4 T	207	2.6 (compared to mid-field)

	9.4 T	76	2.4 (compared to high-field)
$Gd_3N@C_{80}(PEG)(OH)_x$, PEG M.W.= 350	0.35 T	227	3.4 (compared to low-field)
	2.4 T	237	2.9 (compared to mid-field)
	9.4 T	68.2	2.2 (compared to high-field)
$Gd_3N@C_{80}(PEG)(OH)_x$, PEG M.W.= 750	0.35 T	152	2.3 (compared to low-field)
	2.4 T	232	2.9 (compared to mid-field)
	9.4 T	63.3	2.0 (compared to high-field)
$Gd_3N@C_{80}(PEG)(OH)_x$, PEG M.W.= 2000	0.35 T	130	1.9 (compared to low-field)
	2.4 T	158	2.0 (compared to mid-field)
	9.4 T	41.9	1.4 (compared to high-field)
$Gd_3N@C_{80}(PEG)(OH)_x$, PEG M.W.= 5000	0.35 T	107	1.6 (compared to low-field)
	2.4 T	139	1.7 (compared to mid-field)
	9.4 T	52.5	1.7 (compared to high-field)
$Gd_3N@C_{80}O_{11}(OH)_{21}$ (current work)	0.47 T	137	2.0 (compared to low-field)
	1.4 T	140	1.7 (compared to mid-field)
	9.4 T,	58	1.9 (compared to high-field)
$Gd_3N@C_{84}O_6(OH)_{28}$ (current work)	0.47 T	170	2.5 (compared to low-field)
	1.4 T	173	2.1 (compared to mid-field)
	9.4 T	63	2.0 (compared to high-field)

2.7.2 Relaxivity comparison of $Gd_3N@C_{80}$ and $Gd_3N@C_{84}$ metallofullerenols

One major contributing factor for the significantly higher relaxivity of the $Gd_3N@C_{84}$ metallofullerenols is the lower carbonyl content. Previous fullerene hydroxylation showed that carbonyl groups are easier to form under acidic conditions;[27] however, carbonyl groups can also form in lower amounts under basic or neutral conditions.[28] XPS data revealed that carbonyl

formation is less favored for $Gd_3N@C_{84}$ than for $Gd_3N@C_{80}$, likely related to the low symmetry and special egg shape caused by the pentalene unit. One reaction mechanism accounting for this difference is related to the hopping of negative charges. Nucleophilic attack from a hydroxyl group creates a carbanionic site on the cage surface, which can be readily oxidized by oxygen.[29] The involvement of oxygen had been confirmed by an argon-protected reaction that led to very low yield.[28] Before oxidation, the negative charge can be dispersed over the fullerene cage via the π-conjugated system to form enolic groups, which are potential sources of carbonyl formation via enol-keto tautomerization. An example of such a rearrangement is illustrated in Figure 14. For $Gd_3N@C_{84}$ which has an elliptical shape with enhanced dipole moment,[16,19] the electron density is unevenly distributed on the cage, and it is reasonable to expect the nucleophilic reaction sites are "crowded" on parts of the cage with lower electron density, rather than uniformly spread out as in the case of $Gd_3N@C_{80}$, which is expected to lower the negative charge hopping and limit carbonyl formation.

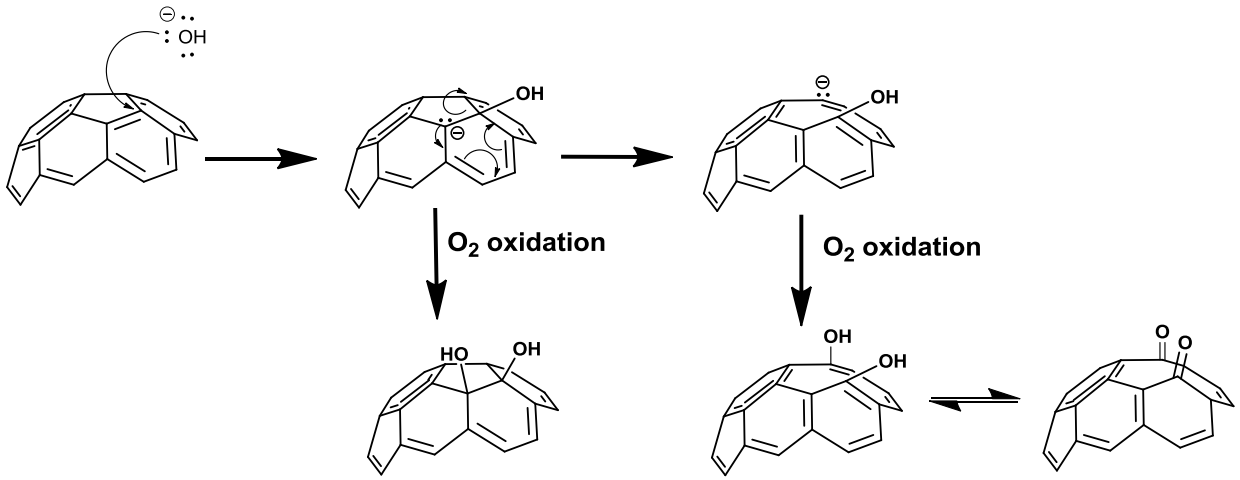

Figure 14. Proposed mechanism for carbonyl formation during the hydroxylation procedure of metallofullerenes.

2.8 Conclusion

In this chapter, the synthesis, characterization and application as MRI contrast agents of $Gd_3N@C_{80}$ and $Gd_3N@C_{84}$ metallofullerenols are presented. The relaxivity of $Gd_3N@C_{84}$ is significantly higher than the $Gd_3N@C_{80}$ under identical conditions. The ellipsoidal shape and the pentalene motif of $Gd_3N@C_{84}$ system could be the main factors that contribute to the difference in functionalization, aggregation and relaxivity in comparison with the $Gd_3N@C_{80}$ system. With the increasing yield of EMFs, $Gd_3N@C_{84}$ and other pentalene-containing metallofullerenes can evolve as excellent candidates for next-generation MRI contrast and theranostic agents.

2.9 **Reference**

(1) Caravan, P.; Ellison, J. J.; McMurry, T. J.; Lauffer, R. B.: Gadolinium(III) Chelates as MRI Contrast Agents: Structure, Dynamics, and Applications. *Chemical Reviews* **1999**, *99*, 2293-2352.

(2) Mikawa, M.; Kato, H.; Okumura, M.; Narazaki, M.; Kanazawa, Y.; Miwa, N.; Shinohara, H.: Paramagnetic water-soluble metallofullerenes having the highest relaxivity for MRI contrast agents. *Bioconjugate Chemistry* **2001**, *12*, 510-514.

(3) Kato, H.; Kanazawa, Y.; Okumura, M.; Taninaka, A.; Yokawa, T.; Shinohara, H.: Lanthanoid Endohedral Metallofullerenols for MRI Contrast Agents. *Journal of the American Chemical Society* **2003**, *125*, 4391-4397.

(4) Bolskar, R. D.; Benedetto, A. F.; Husebo, L. O.; Price, R. E.; Jackson, E. F.; Wallace, S.; Wilson, L. J.; Alford, J. M.: First Soluble $M@C_{60}$ Derivatives Provide Enhanced Access to Metallofullerenes and Permit in Vivo Evaluation of $Gd@C_{60}[C(COOH)_2]_{10}$ as a MRI Contrast Agent. *Journal of the American Chemical Society* **2003**, *125*, 5471-5478.

(5) Tóth, É.; Bolskar, R. D.; Borel, A.; González, G.; Helm, L.; Merbach, A. E.; Sitharaman, B.; Wilson, L. J.: Water-Soluble Gadofullerenes: Toward High-Relaxivity, pH-Responsive MRI Contrast Agents. *Journal of the American Chemical Society* **2004**, *127*, 799-805.

(6) Sitharaman, B.; Bolskar, R. D.; Rusakova, I.; Wilson, L. J.: $Gd@C_{60}[C(COOH)_2]_{10}$ and $Gd@C_{60}(OH)_x$: Nanoscale Aggregation Studies of Two Metallofullerene MRI Contrast Agents in Aqueous Solution. *Nano Letters* **2004**, *4*, 2373-2378.

(7) Stevenson, S.; Rice, G.; Glass, T.; Harich, K.; Cromer, F.; Jordan, M. R.; Craft, J.; Hadju, E.; Bible, R.; Olmstead, M. M.; Maitra, K.; Fisher, A. J.; Balch, A. L.; Dorn, H. C.: Small-bandgap endohedral metallofullerenes in high yield and purity. *Nature* **1999**, *401*, 55-57.

(8) Zhang, J.; Stevenson, S.; Dorn, H. C.: Trimetallic Nitride Template Endohedral Metallofullerenes: Discovery, Structural Characterization, Reactivity, and Applications. *Accounts of Chemical Research* **2013**.

(9) Fatouros, P. P.; Corwin, F. D.; Chen, Z.-J.; Broaddus, W. C.; Tatum, J. L.; Kettenmann, B.; Ge, Z.; Gibson, H. W.; Russ, J. L.; Leonard, A. P.; Duchamp, J. C.; Dorn, H. C.: In vitro and in vivo imaging studies of a new endohedral metallofullerene nanoparticle. *Radiology* **2006**, *240*, 756-764.

(10) Zhang, E.-Y.; Shu, C.-Y.; Feng, L.; Wang, C.-R.: Preparation and Characterization of Two New Water-Soluble Endohedral Metallofullerenes as Magnetic Resonance Imaging Contrast Agents. *The Journal of Physical Chemistry B* **2007**, *111*, 14223-14226.

(11) Shu, C.; Corwin, F. D.; Zhang, J.; Chen, Z.; Reid, J. E.; Sun, M.; Xu, W.; Sim, J. H.; Wang, C.; Fatouros, P. P.; Esker, A. R.; Gibson, H. W.; Dorn, H. C.: Facile Preparation of a New Gadofullerene-Based Magnetic Resonance Imaging Contrast Agent with High (1)H Relaxivity. *Bioconjugate Chemistry* **2009**, *20*, 1186-1193.

(12) MacFarland, D. K.; Walker, K. L.; Lenk, R. P.; Wilson, S. R.; Kumar, K.; Kepley, C. L.; Garbow, J. R.: Hydrochalarones: A Novel Endohedral Metallofullerene Platform for Enhancing Magnetic Resonance Imaging Contrast. *Journal of Medicinal Chemistry* **2008**, *51*, 3681-3683.

(13) Zhang, J.; Fatouros, P. P.; Shu, C.; Reid, J.; Owens, L. S.; Cai, T.; Gibson, H. W.; Long, G. L.; Corwin, F. D.; Chen, Z.-J.; Dorn, H. C.: High Relaxivity Trimetallic Nitride (Gd(3)N) Metallofullerene MRI Contrast Agents with Optimized Functionality. *Bioconjugate Chemistry* **2010**, *21*, 610-615.

(14) Shultz, M. D.; Wilson, J. D.; Fuller, C. E.; Zhang, J.; Dorn, H. C.; Fatouros, P. P.: Metallofullerene-based Nanoplatform for Brain Tumor Brachytherapy and Longitudinal Imaging in a Murine Orthotopic Xenograft Model. *Radiology* **2011**, *261*, 136-143.

(15) Fatouros, P. P.; Shultz, M. D.: Metallofullerenes: a new class of MRI agents and more? *Nanomedicine* **2013**, *8*, 1853-1864.

(16) Zuo, T.; Walker, K.; Olmstead, M. M.; Melin, F.; Holloway, B. C.; Echegoyen, L.; Dorn, H. C.; Chaur, M. N.; Chancellor, C. J.; Beavers, C. M.; Balch, A. L.; Athans, A. J.: New egg-shaped fullerenes: non-isolated pentagon structures of $Tm_3N@C_s(51365)$-C_{84} and $Gd_3N@C_s(51365)$-C_{84}. *Chemical Communications* **2008**, 1067-1069.

(17) Stevenson, S.; Phillips, J. P.; Reid, J. E.; Olmstead, M. M.; Rath, S. P.; Balch, A. L.: Pyramidalization of Gd_3N inside a C_{80} cage. The synthesis and structure of Gd3N@C-80. *Chemical Communications* **2004**, 2814-2815.

(18) Fu, W.; Xu, L.; Azurmendi, H.; Ge, J.; Fuhrer, T.; Zuo, T.; Reid, J.; Shu, C.; Harich, K.; Dorn, H. C.: ^{89}Y and ^{13}C NMR Cluster and Carbon Cage Studies of an Yttrium Metallofullerene Family, $Y_3N@C_{2n}$ (n=40-43). *Journal of the American Chemical Society* **2009**, *131*, 11762-11769.

(19) Zhang, J.; Bearden, D. W.; Fuhrer, T.; Xu, L.; Fu, W.; Zuo, T.; Dorn, H. C.: Enhanced Dipole Moments in Trimetallic Nitride Template Endohedral Metallofullerenes with the Pentalene Motif. *Journal of the American Chemical Society* **2013**, *135*, 3351-3354.

(20) Fu, W.; Zhang, J.; Fuhrer, T.; Champion, H.; Furukawa, K.; Kato, T.; Mahaney, J. E.; Burke, B. G.; Williams, K. A.; Walker, K.; Dixon, C.; Ge, J.; Shu, C.; Harich, K.; Dorn, H. C.: $Gd_2@C_{79}N$: Isolation, Characterization, and Monoadduct Formation of a Very Stable Heterofullerene with a Magnetic Spin State of S=15/2. *Journal of the American Chemical Society* **2011**, *133*, 9741-9750.

(21) Husebo, L. O.; Sitharaman, B.; Furukawa, K.; Kato, T.; Wilson, L. J.: Fullerenols Revisited as Stable Radical Anions. *Journal of the American Chemical Society* **2004**, *126*, 12055-12064.

(22) Shu, C. Y.; Gan, L. H.; Wang, C. R.; Pei, X. L.; Han, H. B.: Synthesis and characterization of a new water-soluble endohedral metallofullerene for MRI contrast agents. *Carbon* **2006**, *44*, 496-500.

(23) Shu, C.-Y.; Wang, C.-R.; Zhang, J.-F.; Gibson, H. W.; Dorn, H. C.; Corwin, F. D.; Fatouros, P. P.; Dennis, T. J. S.: Organophosphonate Functionalized Gd@C82 as a Magnetic Resonance Imaging Contrast Agent. *Chemistry of Materials* **2008**, *20*, 2106-2109.

(24) Laus, S.; Sitharaman, B.; Tóth, É.; Bolskar, R. D.; Helm, L.; Asokan, S.; Wong, M. S.; Wilson, L. J.; Merbach, A. E.: Destroying Gadofullerene Aggregates by Salt Addition in Aqueous Solution of $Gd@C_{60}(OH)_x$ and $Gd@C_{60}[C(COOH_2)]_{10}$. *Journal of the American Chemical Society* **2005**, *127*, 9368-9369.

(25) Funasaka, H.; Sakurai, K.; Oda, Y.; Yamamoto, K.; Takahashi, T.: Magnetic properties of $Gd@C_{82}$ metallofullerene. *Chemical Physics Letters* **1995**, *232*, 273-277.

(26) Kitaura, R.; Okimoto, H.; Shinohara, H.; Nakamura, T.; Osawa, H.: Magnetism of the endohedral metallofullerenes M@C_{82} (M=Gd,Dy) and the corresponding nanoscale peapods: Synchrotron soft x-ray magnetic circular dichroism and density-functional theory calculations. *Physical Review B* **2007**, *76*, 172409.

(27) Kato, H.; Suenaga, K.; Mikawa, W.; Okumura, M.; Miwa, N.; Yashiro, A.; Fujimura, H.; Mizuno, A.; Nishida, Y.; Kobayashi, K.; Shinohara, H.: Syntheses and EELS characterization of water-soluble multi-hydroxyl Gd@C_{82} fullerenols. *Chemical Physics Letters* **2000**, *324*, 255-259.

(28) Li, J.; Takeuchi, A.; Ozawa, M.; Li, X. H.; Saigo, K.; Kitazawa, K.: C_{60} fullerol formation catalyzed by quaternary ammonium hydroxides. *Journal of the Chemical Society-Chemical Communications* **1993**, 1784-1785.

(29) Russell, G. A.; Bemis, A. G.: The Oxidation of Carbanions. I. Oxidation of Triaryl Carbanions and Other Tertiary Carbanions1. *Journal of the American Chemical Society* **1966**, *88*, 5491-5497.

Chapter 3 Magnetic Resonance Imaging Studies of Unfunctionlized $Gd_3N@C_{80}$ in Oleic Acid

3.1 Introduction

With the broad application of the MRI techniques, a variety of different contrast agents are needed to exploit their potential. As shown in previous chapters, the aqueous phase MRI contrasts are undergoing rapid development, and gadolinium based EMFs have been functionalized in a variety of ways to provide a sufficient hydrophilic character to the metallofullerene surface to enable water solubility for next generation MRI contrast agents.

However, there have been limited studies reported devoted to hydrophobic MRI contrast agents. While most MRI contrast agents requires water solubility, some hydrophobic MRI probes can be delivered in nanocarriers such as liposomes, microemulsions, micelles, and synthetic solid lipid nanoparticles,[1] which triggers increasing interest for new MRI contrast agents that have surfaces with greater hydrophobic and lipophilic character.

As efficient and promising future MRI contrast agents, gadolinium based EMFs are naturally soluble in many organic solvents, such as dichlorobenzene, toluene, carbon disulfide and they have decent solubility in oleic acid and its esters. Therefore, they have the potential to be used as MRI contrast agents even without functionalization. In addition, fullerene cages are somewhat beneficial to human health. For example, C_{60} is added to many skin care products for its radical scavenging ability.[2] Moreover, a recent study suggested that oral administration of C_{60} in olive oil solution (0.8 mg/mL) almost doubled the lifespan of rats compared to the control group.[3] Although the mechanism for rat life-span increase remains unclear, this study provides the impetus to study the relaxivity and biological effects of the unfunctionalized Gd EMFs. In this

chapter, I present a preliminary study of $Gd_3N@C_{80}$ in oleic acid, whose ester is one of the major components in olive oil, as a potential MRI contrast agent.

3.2 Experimental section

A $Gd_3N@C_{80}$ sample was purchased from LUNA Nanoworks and used without purification. To make a solution, 1.8 mg of $Gd_3N@C_{80}$ was dissolved in 20 mL of oleic acid and the mixture was sonicated for 1 hour to afford a stable solution that remained clear without precipitates in 14 days. The concentration of the parent solution was 0.090 mg/mL, or 0.062 mM. A series of the oleic acid solutions were made from the parent solution. In similar fashion, oleic acid solutions of C_{60} were prepared as controls. NMR relaxation measurements were performed on Bruker Minispec mq20 (0.47 T) and mq60 (1.41 T) analyzers in 5 mm NMR tubes. The spin-lattice relaxation time T_1 was measured by the inversion-recovery method. The spin-spin relaxation time T_2 was measured using an incremented echo-train CPMG pulse sequence.

3.3 Relaxivity values

As noted in previous chapter, relaxivity is defined by the equation:

$$\frac{1}{T_{i,\ obs}} = \frac{1}{T_{i,\ OA}} + \frac{1}{T_{i,\ para}} = \frac{1}{T_{i,\ OA}} + r_i[M] \quad i = 1, 2$$

where T_1 and T_2 are longitudinal and transverse relaxation time, respectively. The relaxation rate (reciprocal of relaxation time) is determined by both diamagnetic (oleic acid) and paramagnetic (contrast agent) species, and the ratio of paramagnetic relaxation rate to the concentration is the relaxivity of the paramagnetic compound, which can be experimentally obtained by the slope of ($1/T_i$) vs. concentration of the paramagnetic contrast agents.

The relaxation time vs. concentration plots are displayed in Figures 1 and Figure 2, for 20 MHz (0.47 T) and 60 MHz (1.4 T) respectively. For oleic acid, the protons are non-equivalent; therefore, each relaxation time obtained represents an average of different protons. The relaxivity results obtained from the plots are displayed in Table 1.

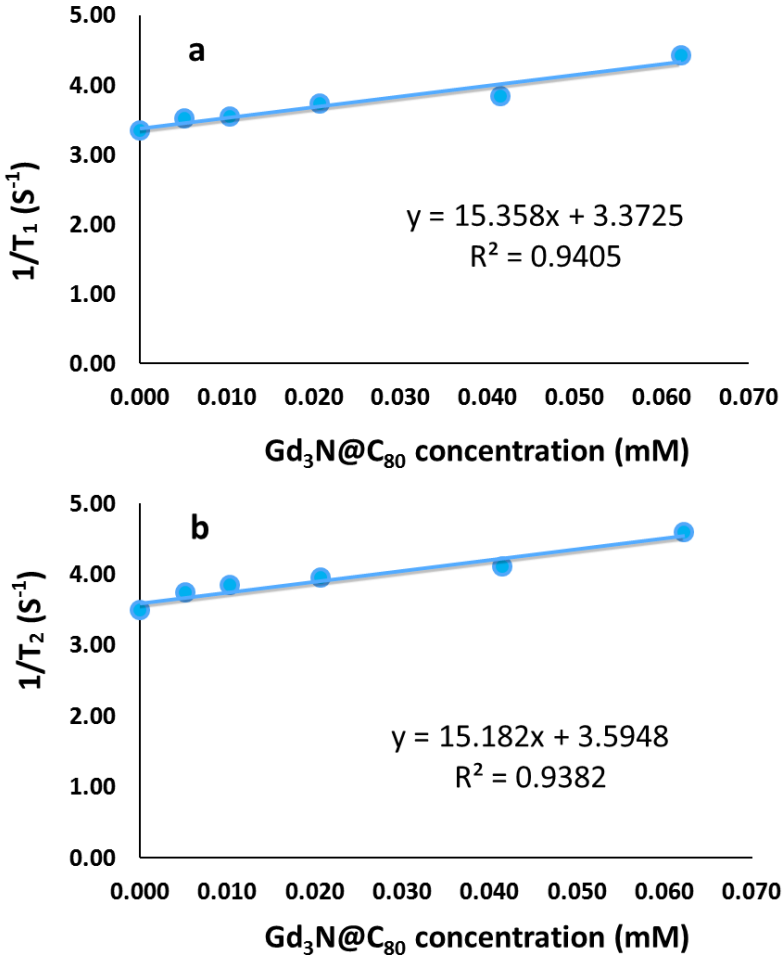

Figure 1. T_1 (a) and T_2 (b) measurements of $Gd_3N@C_{80}$ in oleic acid on a 20 MHz (0.47 T) instrument.

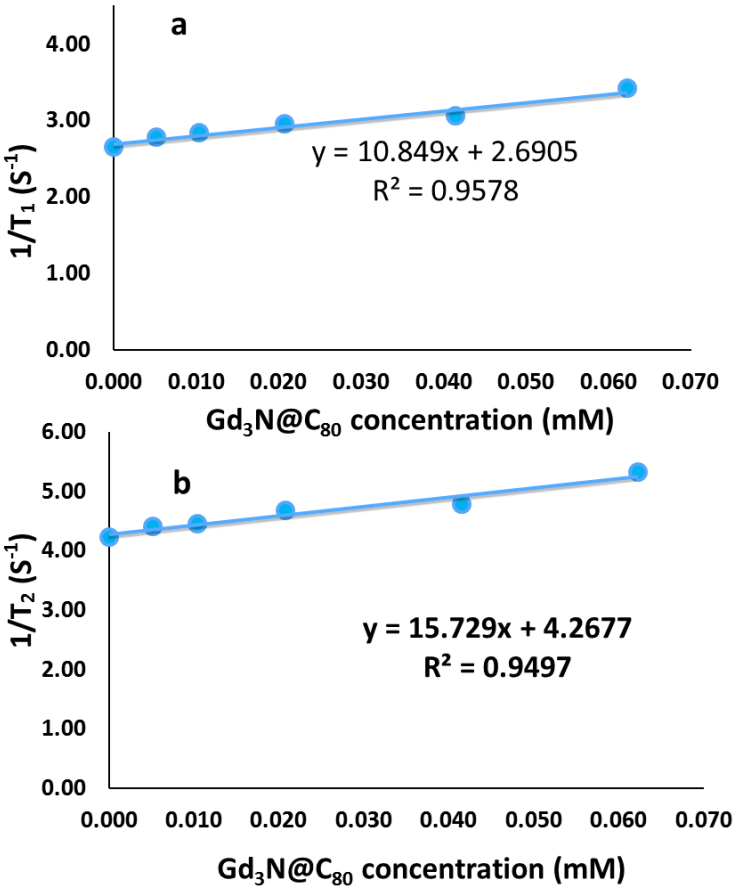

Figure 2. T_1 (a) and T_2 (b) measurements of $Gd_3N@C_{80}$ in oleic acid on a 60 MHz (1.4 T) instrument.

Table 1. Relaxivity values of oleic solution of $Gd_3N@C_{80}$.

0.47 T			1.4 T		
r_1 ($mM^{-1}S^{-1}$)	r_2 ($mM^{-1}S^{-1}$)	r_2/r_1	r_1 ($mM^{-1}S^{-1}$)	r_2 ($mM^{-1}S^{-1}$)	r_2/r_1
15	15	1.0	11	16	1.5

Also, the oleic acid solutions of C_{60} were prepared as a control by adding 1.3 mg of C_{60} to 20 ml of oleic acid, followed by subsequent dilutions, and the relaxation times of these solutions were obtained on the 20 MHz (0.47 T) instrument, as shown in Figure 3. From the data it can be concluded that empty C_{60} fullerene cage did not decrease the relaxation times of the solution, and there was no linear relationship between the relaxation rate and the concentration of fullerene. A former linear trendline was obtained based on current data. The very low R^2 values and negative slopes suggested that the relaxivity was caused by Gd^{3+} encapsulated inside the fullerene cage instead of the cage itself.

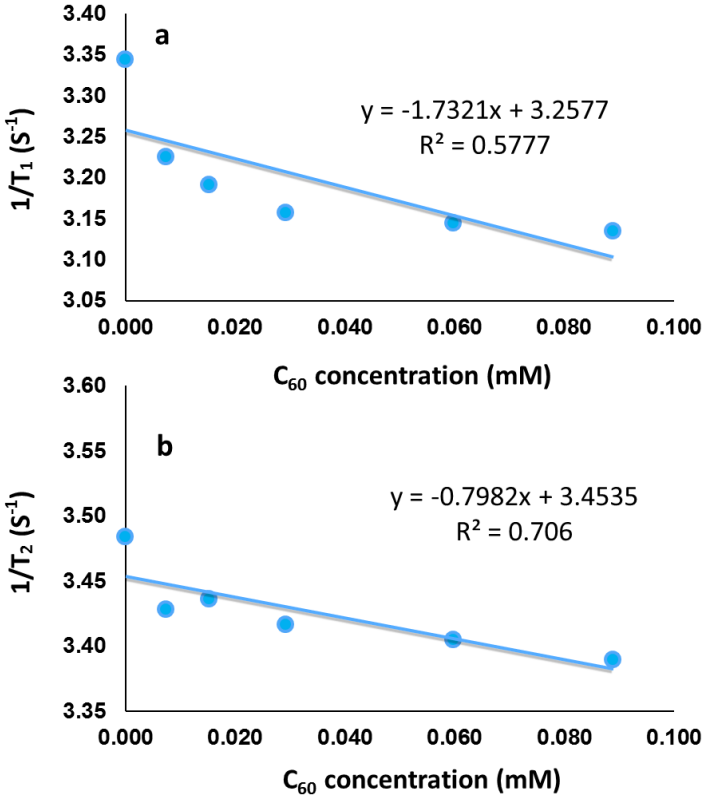

Figure 3. T_1 (a) and T_2 (b) measurements of C_{60} in oleic acid on a 20 MHz (0.47 T) instrument.

3.4 *In vitro* MRI study of $Gd_3N@C_{80}$ in oleic acid

Since the $Gd_3N@C_{80}$ in oleic acid samples were found to exhibit relaxivity, a visual test of the unfunctionalized metallofullerene in oleic acid as hydrophobic MR contrast agents was performed in comparison with pure oleic acid on a Siemens 3 T clinical MRI instrument (Fig. 4). The images were obtained in the Stephen LaConte laboratory at VTCRI. $Gd_3N@C_{80}$ in oleic acid was prepared in three different dilution concentrations. Along with pure oleic acid, the solutions were scanned under inversion recovery sequence with inversion time changing from 23 ms to 1000 ms. Images obtained at inversion time 23 ms and 100 ms are presented in Figure 4. In Figure 4c and 4g, the oleic acid solution of $Gd_3N@C_{80}$ in the highest concentration (0.062 mM) was not as bright as the ones in lower concentration at both inversion times (23 and 1000 ms). It was found afterwards that solids had precipitated out of the solution during the experiment. In this case, 4c and 4g were not informative in the study of contrast ability of $Gd_3N@C_{80}$ in oleic acid samples and were therefore excluded from the following discussion. Distinguishable signal differences were observed at both inversion times between $Gd_3N@C_{80}$ in oleic acid of different concentrations. (0.0052 mM and 0.021 mM, Fig. 4a,b,e,f) The solution in higher concentration appeared to be brighter. Such trend also showed up at other inversion time (images not showing here), indicating the contrast function of $Gd_3N@C_{80}$ was proportional to the concentration of the metallofullerene, which is consistent with the observations on hydrophilic metallofullerene based MRI contrast agents. However, comparisons between $Gd_3N@C_{80}$ in oleic acid and pure oleic acid were different than expected. The pure oleic acid sample turned out to be the brightest among all at both inversion time, though very close to the 0.021 mM $Gd_3N@C_{80}$ sample. (Fig. 4b vs 4d, Fig. 4f vs 4h) One possible explanation is that dissolve paramagnetic oxygen is an interference contaminate at these low concentrations. As a common paramagnetic substance, oxygen dissolving in oleic acid would clearly affect the MRI behavior of the samples. A

degasing step before future MR imaging on $Gd_3N@C_{80}$ in oleic acid could resolve this interference question.

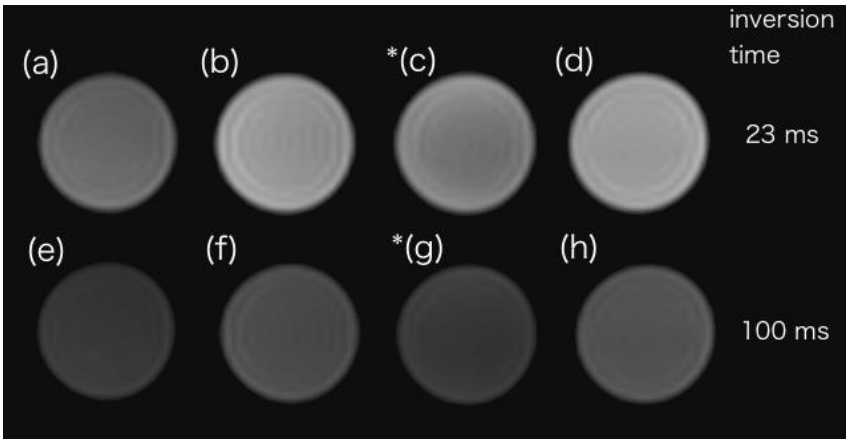

Figure 4. T_1-weighted MR imaging at 3 T with $Gd_3N@C_{80}$ in oleic acid under inversion recovery sequence. Top line, inversion time = 23 ms, from left to right: (a) 0.0052 mM $Gd_3N@C_{80}$ in oleic acid, (b) 0.021 mM $Gd_3N@C_{80}$ in oleic acid, (c) 0.062 mM $Gd_3N@C_{80}$ in oleic acid, (d) pure oleic acid. Bottom line, inversion time = 100 ms, from left to right: (e) 0.0052 mM $Gd_3N@C_{80}$ in oleic acid, (f) 0.021 mM $Gd_3N@C_{80}$ in oleic acid, (g) 0.062 mM $Gd_3N@C_{80}$ in oleic acid, (h) pure oleic acid. *Data points (c) and (g) are not informative due to solids precipitating out during the experiment.

3.5 Discussion

The relaxivity of $Gd_3N@C_{80}$ oleic acid solutions has been obtained. At both 0.47 T and 1.4 T, $Gd_3N@C_{80}$ solutions showed moderate but promising relaxivity values, namely, r_1=10-15 $mM^{-1}S^{-1}$, r_2=~15 $mM^{-1}S^{-1}$, which are comparable to current commercial contrast agents even only considering "per Gd" relaxivity (one third of the relaxivity for TNT EMF molecules). This suggests that gadolinium-based TNT EMFs are potentially usable MRI contrast agents even

without functionalization. The control experiment on C_{60} proved that the relaxation is due to the endohedral gadolinium ions, not the fullerene cage.

However, it is notable that the preliminary relaxivity study has some limitations. First, the relaxation times and relaxivity values only show an average of different protons in oleic acid, which consist of mainly similar, but still non-equivalent aliphatic protons, plus vinyl and carboxyl protons. This means the relaxivity is not necessarily always consistent with the real MRI signal intensities in oleic acid media. Also, the experimental uncertainty was increased, as can be seen that the linear relationship for the plots (Figures 1, 2) are not as good (r^2=0.94-0.95) compared to those for the water-soluble derivatives (r^2>0.99). In addition, the 20 MHz result showed an r_2 about the same as r_1, which could be caused by experimental uncertainty as well.

The MR imaging results of the oleic acid solutions partially supported the relaxation effect of the $Gd_3N@C_{80}$ molecules. Higher concentrations of $Gd_3N@C_{80}$ had led to brighter images. However, the brightness of pure oleic acid is contradictory to this conclusion. As discussed above, the higher brightness of pure oleic acid sample may be related to dissolved oxygen, but other reasons are also possible. Further careful experiments with degassed samples are needed to help investigate the oleic acid based system.

3.6 Reference

(1) Aime, S.; Castelli, D. D.; Crich, S. G.; Gianolio, E.; Terreno, E.: Pushing the Sensitivity Envelope of Lanthanide-Based Magnetic Resonance Imaging (MRI) Contrast Agents for Molecular Imaging Applications. *Accounts of Chemical Research* **2009**, *42*, 822-831.

(2) Bakry, R.; Vallant, R. M.; Najam-ul-Haq, M.; Rainer, M.; Szabo, Z.; Huck, C. W.; Bonn, G. K.: Medicinal applications of fullerenes. *International Journal of Nanomedicine* **2007**, *2*, 639-649.

(3) Baati, T.; Bourasset, F.; Gharbi, N.; Njim, L.; Abderrabba, M.; Kerkeni, A.; Szwarc, H.; Moussa, F.: The prolongation of the lifespan of rats by repeated oral administration of [60]fullerene. *Biomaterials* **2012**, *33*, 4936-4946.

Chapter 4 Future Work

The field of metallofullerenes is growing fast, but for gadolinium based EMFs to become mature MRI contrast agents, there are many challenges yet to be overcome. In this chapter I propose several possible projects for future work.

First, the functionalization toolbox should be expanded. So far, all the reported gadolinium EMF derivatives were functionalized as a mixture of multi-functionalized EMFs, and their formulas represented an average number of functional groups. This is due to the necessity of multiple functional groups to really achieve sufficient water solubility and relaxivity. However, for a drug to be approved by FDA, a certain molecule with definitively elucidated structure is required in most cases. One challenge in the EMF field is how to make well-defined multi-functionalized gadolinium EMFs that have high relaxivity, for a better fundamental understanding, experiment reproducibility and easier drug approval.

Second, an effective targeting methodology has not been established. Multi-step functionalization can introduce a variety of biological structures to the EMFs which realize effective targeting. Currently there has been some success in introducing IL-13 peptide onto EMFs, but a deeper understanding about IL-13, as well as other targeting agents which may require systemic functionalization approaches, are still needed.

Third, the relationship between cage symmetry and relaxivity should be explored further. In this thesis I have demonstrated that the non-IPR $Gd_3N@C_{84}$ has higher relaxivity than $Gd_3N@C_{80}$. With increasing availability of a variety of gadolinium EMFs, a full investigation of the cage symmetry (especially the non-IPR cages) and relaxivity

relationship will be helpful to find the ideal cage to host the gadolinium ions for MRI purposes.

Fourth, the health effect of metallofullerenes has not been established. Fullerene C_{60} has been reported to significantly increase the lifespan of rats when fed together with olive oil, and this makes the animal experiments on EMFs are very intriguing. Such experiments can start with smaller animals, such as mice, or even smaller, fruit flies. In the experimental group, the animals are fed with EMF (e.g. gadolinium EMFs) solutions in olive oil or similar compounds, while the control group is only fed the solvent without metallofullerenes. The first part should be a longevity experiment which reveals the toxic and health effects of unfunctionalized EMFs. The second part should be a biodistribution study which can be done by using ICP to measure the metal (e.g. gadolinium) concentrations.

In all, gadolinium based endohedral metallofullerenes and their derivatives have amazing properties that will lead to excellent MRI contrast agents. This is an attractive area that worth further exploration.